Antenna Bandwidth and Radiation Control by Topology and use of Non-Conductive Materials

by

Hatim A. Bukhari

A dissertation submitted in partial fulfillment
of the requirements for the degree of
Doctor of Philosophy
(Electrical Engineering)
in The University of Michigan
2016

Doctoral Committee:

Professor Kamal Sarabandi, Chair
Associate Professor Anthony Grbic
Professor Jerome Lynch
Professor Eric Michielssen

To God,

then to my mother and father with love and gratitude.

ACKNOWLEDGMENT

First, I would like first to thank God for giving me the power to pursue my dreams and his guidance. I could never have accomplished my Ph.D. without the faith I have in you, the Almighty. I would also like to thank my parents, brother, and sisters for all their love and support throughout the years that I have been away from them, but especially my mother. She was my motivation to pursue my Ph.D.

I have had the privilege of having Professor Kamal Sarabandi as my research advisor and dissertation committee chair. Kamal, I want to thank you for your unlimited support, guidance, patience and mentorship in both research and personal life. Your dedication and passion about research has truly inspired me. Additionally, I would like to thank my other committee members, Dr. Anthony Grbic, Dr. Eric Michielssen, and Dr. Jerome Lynch for their guidance and support towards the completion of my Ph.D. work.

I would like to express my gratitude and appreciation to many amazing teachers and mentors I have had at the University of Michigan and King Abulaziz City for Science and Technology (KACST). I would like to thank in particular Dr. Sami Alhumaidi, my former boss at KACST, for believing in me and supporting me throughout the years I was there and also towards my Ph.D. here at the University of Michigan.

I would like to thank all my friends and colleagues. Adel Elsherbini, thank you for your help and sharing your knowledge with me. Mani Kashanianfard and Xiuzhang Cai, I am thankful for your help in the lab when I needed it. Brian Tierney and Gurkan Gok, I would like to thank you

both for helping me in fabricating several of my antennas in your lab. Dr. Adib Nashashibi, I am thankful for your advice and assistance on any aspect related to measurements in the lab. Dr. Waleed Alomar and Amr Ibrahim, I would like to thank you both for your support, sharing your knowledge and being my office mates throughout the years. Michael Benson, I am thankful for your effort in reviewing my English grammar in some of my papers.

I had the opportunity to interact with many people within the university and outside the school. I have met many outstanding researchers, students and intelligent people during my Ph.D. period. I would like to thank all my colleagues, research groups, office mates, and all my friends. I would have never reached this stage without your support and encouragement. Thank you all for all the good times we have had.

Hatim Bukhari

November 23, 2015

Table of Contents

LIST OF FIGURES

ABSTRACT

Antenna Bandwidth and Radiation Control by Topology and use of Non-Conductive Materials

by

Hatim A. Bukhari

Chair: Kamal Sarabandi

The demand for ultra-wideband (UWB) antennas have been on the rise in the last decade. There are many different systems and devices such as ground penetrating radars (GPRs) and wireless communications where such antennas find very unique applications. Many topologies and configurations have been studied and reported in designing UWB antennas. These topologies are corresponding to radiation pattern, polarization, and band of operation. In addition, in low frequencies, such as in VHF and UHF bands, the size of the antenna becomes a major factor that must be taken into consideration. A portion of this thesis focuses on the design of novel UWB antennas.

A new approach in design of a cavity-backed coupled sectorial loop antenna (CB-CSLA) with directional radiation pattern is presented. This antenna is backed by a short cylindrical cavity with a special modal suppressing septum to accomplish a unidirectional radiation pattern while

maintaining a very wide bandwidth. A prototype is fabricated to validate the design and it is shown that a CB-CSLA with diameters of λ/4 and height of λ/5 can provide a fabricated bandwidth of 38% in addition to a front to back ratio of 15dB.Another approach, more applicable to ground penetrating radars, based on dielectric loaded multi-resonant slot antenna is also presented. Unidirectional radiation is achieved by a symmetrically loading the slot radiators. Since the slot length is reduced, radiation is preferentially aimed towards the dielectric superstrate. By gradually changing the index of refraction, the radiation from the dielectric back to the surrounding medium is facilitated. A prototype with dimension of 0.28λ by 0.2λ by 0.07λ is fabricated and shown to have a bandwidth of 35.5% and a front to back ratio of 12dB.

For the new 700MHz band considered for wireless communication applications, a novel planar wideband slot antenna is designed. The slot antenna size is reduced from the traditional λ/2 slot to λ/4. Then parasitic coupling, using a number of λ/4 slot elements appropriately positioned around the driving element, and direct feeding are used to increase the bandwidth.

For communication applications, a novel miniaturized impedance matched antenna with an omnidirectional horizontally polarized radiation pattern is then presented. The antenna structure resembles a circular loop formed by a circular array of shunt miniaturized n-fold resonant dipole antennas which is referred to as a miniature composite wire-loop antenna (MCWLA). This antenna has a diameter of λ/9 and a height of less than λ/500. The measured gain and radiation efficiency are, respectively, 0dBi and 67%.

Chapter 1:
Introduction

1.1 Motivation

In radio communication, the information rate over a wireless channel is directly related to the available bandwidth and the energy per bit of information. The propagation environment that affects signal attenuation and multi-path characteristics is also an important parameter in determining the data rate. Ultra-Wideband (UWB) communication systems are often considered for high data rate systems in conjunction with Code Division Multiple Access (CDMA) modulation [1] and [2]. Such systems allow for sharing the available spectrum among multiple users using specific code that is orthogonal to other codes. This scheme also allows for transceivers to radiate signal whose power spectral density is lower than the noise floor. It also allows to transmit information in a specific signal over a greater bandwidth than the original signal. One of the most widespread CDMA method is the Pseudo-random noise sequence. One of the advantages of CDMA systems over the Frequency Division Multiple Access (FDMA) and Time Division Multiple Access (TDMA) systems is the ability to use the available bandwidth more efficiently. However, a disadvantage of using the CDMA is the Multi Access Interference (MAI) [2] and [3]. This scheme is easy to operate and suitable for different applications.

In radar systems, the dynamic range and range resolution are very important to specify the system performance. There are many applications where high range resolution and high dynamic

range are highly needed such as noise radars, through-the-wall radars, and ground penetrating radars (GPR). In contrast to conventional radars, noise radars use the noise waveform as its transmitting signal. Noise radars have many advantages by using random transmitting signals over other radars [4] and [5]. Noise radars can be used for ultra-wideband applications such as SAR/ISAR mapping [6]-[9]. Noise radars need wide band antennas, noise waveform transmitter, and digital correlation receivers. Figure 1.1 shows the simplest and basic principle of noise rdar. Some radars require a high resolution imaging such as the through-the-wall radars. Through-the-wall radars have become very popular for its ability in detecting objects inside or surrounded by concrete, or other materials [10] and [11]. In order to achieve high resolution, Systems operating with a large frequency bandwidth is highly recommended. However, the attenuation of materials effects the operating frequency range. [12] - [14] suggest that due to the high attenuation of concrete walls, systems operate VHF/UHF band are highly desired.

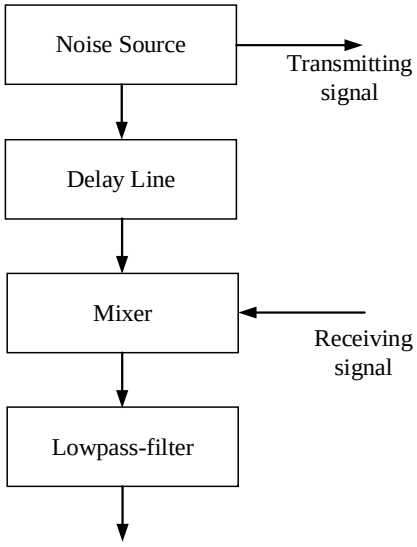

Figure 1.1: Noise radar principle.

Ultra-wideband radars and communications systems are becoming more popular as their applications expand in many areas. They offer advantages in different applications over the narrowband systems. One of the most important and challenging component in all UWB radars and communication systems is the antenna. Many topologies and configurations, corresponding to application specific band of operation, radiation pattern, and polarization, have been studied and reported [15]-[18]. In many applications ultra-wideband operation requirement refers to not only the input impedance bandwidth, but also to consistent radiation pattern and polarization over the band of interest which puts additional constraints in the antenna design. Another challenge in design of such antennas is the size, especially for antennas operating at low frequencies such as in the low VHF through UHF band. At these frequencies antennas with dimensions comparable to a fraction of wavelength at the lowest operating frequency is highly desirable. Such antennas will allow design of compact portable systems such as ground penetrating and through-the-wall imaging radars [13] and [16]. In order to have a better performance of UWB radars, they require antennas to operate across a very large bandwidth with good input impedance matching and radiation pattern characteristics over the operating band of the radar. In such systems, the size and performance of the antenna covering the desired ultra-wideband is usually a limiting factor. Often times the bandwidth performance of antennas is solely determined in terms of their input impedance bandwidth. However, in many radar and some communication applications other antenna characteristics such as radiation pattern, polarization, and phase center must also be maintained over the desired bandwidth. In order to define an antenna as an UWB, there are two available criteria. One criterion is the United States' Federal Communication Commission's (FCC) more recent definition which defines the UWB antenna is to have a fractional bandwidth greater than 20%. An older definition of "Ultra-Wideband" comes from the Defense Advanced Research

Projects Agency (DARPA)'s 1990 report [18] which provides for a fractional bandwidth of over 25%. The Fractional band width is as follow:

$$Fractional\ Bandwidth = 2\frac{f_H - f_L}{f_H + f_L} \geq \begin{cases} 0.20 & FCC \\ 0.25 & DARPA \end{cases} \qquad (1)$$

Where f_H and f_L are the highest and lowest operational frequencies of the antenna respectively. Our interest is focused on antennas with multi-octave bandwidths that have applications in Ground Penetrating Radar (GPR), impulse radars, electromagnetic compatibility (EMC) measurement systems, and wireless communication systems. For many ultra-wideband antennas as the operating frequency increases, the current distribution over the antenna structure changes drastically which can lead to different polarization or radiation patterns. The challenge is to design radiating structures that can not only provide a strong impedance match over a wide bandwidth, but also maintain their direction of maximum radiation and polarization. This can be accomplished if the dimension of the antenna is not a limiting factor. The application of UWB systems with multi-octave bandwidth operation is mainly in the VHF-UHF bands where the wavelength is relatively large. The real estate on most mobile platforms is very limited and thus it is highly desirable to miniaturize the size of the antenna without compromising its performance. Also for all radar applications such, Ground Penetrating Radar (GPR), through-wall imaging, foliage penetration, etc., a directional radiation pattern with significant front-to-back ratio is desired. The limitation in size and the desire for unidirectional radiation pattern further complicates the antenna design. A number of techniques have been developed in the past to design antennas that operate across a very large bandwidth. Traveling wave antennas have been used as wide-band antennas. However, traveling wave antennas have less efficiency, is difficult to match, large dimensions, and high cost. Another technique for designing wide-band antennas is to use multi-resonant radiating structures.

1.2 Applications

1.2.1 Ground Penetrating Radars (GPRs)

Ground Penetrating system is a geophysical technique that uses the radar electromagnetic radiation to detect the reflected signals from the objects underneath the surface. The radar signal is transmitted to the ground by an antenna that is located close to the ground. The reflected signal coming back from the ground can be detected by the same transmitting antenna or by another receiving antenna that is separated from the transmitting antenna (See Figure *1.2*).

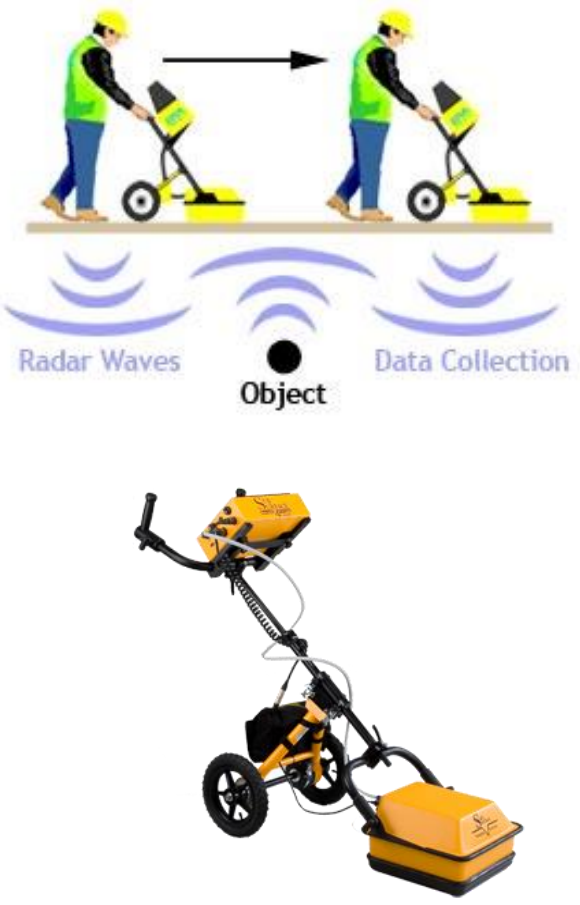

Figure 1.2: Ground penetrating Radar (reproduced from [19] and [20]).

A typical GPR system consists of two antennas, a transmitter and receiver, a computer with a monitor to process the received data, and a power source (see Figure 1.3). The transmitted

electromagnetic waves reflect and scatter from the boundaries between different layers of rock, sand, or objects due to the differences in the electrical properties among them. The electric permittivity and conductivity are the parameters that determine the penetration depth and the reflectivity [21].

GPR needs to operate at lower frequencies for better depth penetration and smaller attenuation losses. It also requires the ultra-wide band system for the following reasons:

a) Enhance the received signal to noise ratio

b) Enhance the range resolution

For deep penetration, GPRs usually operate with center frequencies in the megahertz range but for shallow penetration and better resolution, GPRs operate in gigahertz range, normally in the range of 1 – 6GHz [21]-[24]. Therefore, most of the availabe GPRs operate in the VHF/UHF band. GPRs need smaller antennas in order to provide better mobility, high spatial resolution, and less antenna to target interaction. In all GPR systems, the antenna plays a very important role in the system performance. Providing GPRs with high depth penetration and good resolution requires to design antennas with wide band of operation, good and consistent radiation pattern, and small size. There are many different GPR antenna have been developed and studied [25]-[27]. Most of the popular antennas that are used in GPR applications are the ones can be implemented using planar technology so they can be easily integrated and also has a very low cost.

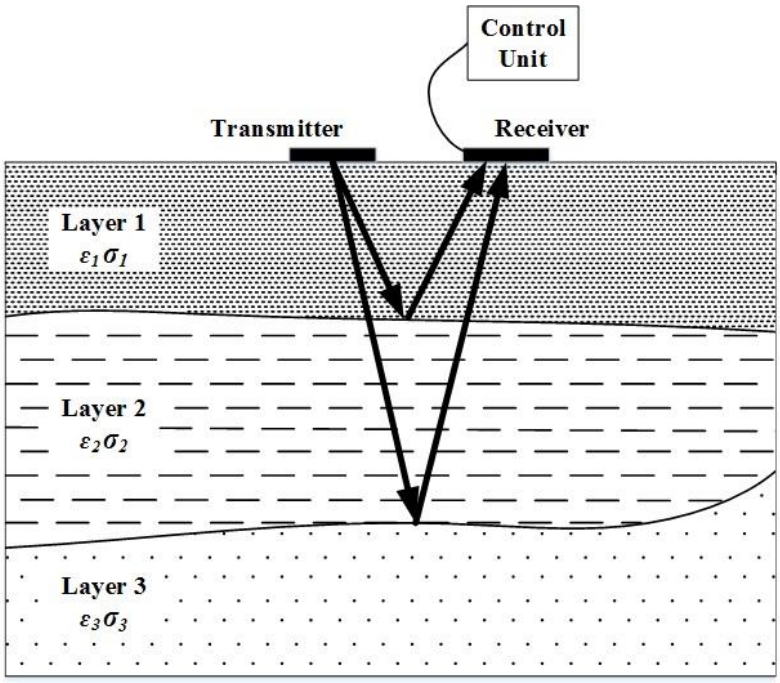

Figure 1.3: Ground penetrating Radar concept.

1.2.2 Wireless systems

Wireless devices became essential part of our daily life routine. The demand for smaller, more efficient wireless devices has received more attention in the last decade. Figure 1.4 shows how cell phone size has evolved throughout the years.

Figure 1.4: Cell phone evolution (reproduced from [28]).

Wireless devices are designed to be capable of receiving many frequencies at the same time and have a consistent performance over the entire band of operation. Most of the wireless system devices have space limitations and since the antenna is considered to be the largest component in most of the wireless systems, therefore, compact antennas covering multiple bands are highly needed and desired. Lot of studies with different approaches in designing miniaturized antennas with efficient radiations and bandwidth that can meet the industry's requirements and can be easily integrated in different communication systems has been documented. This will improve the system reliability, better mobility, and reduce the cost. The relationship between the antenna size and antenna bandwidth and its radiation were studied and reported [29]-[32].

In 2008, the 700MHz spectrum auction started by FCC for the rights to operate in the United States in the 700MHz band for commercial purposes. This band was previously occupied for analog television broadcasting. However, the FCC has decided that this band spectrum is no longer necessary for the television broadcasting due to the digital television transition and its improved spectral efficiency [33]. This transition has free up about 108 MHz of bandwidth that is considered for wireless communication. This band is located between 698MHz to 806 MHz part of the spectrum and referred to as the 700 MHz band. Out of this spectrum 70 MHz is allocated for commercial use, 34 MHz for public safety, and 4 MHz for guard band. It is expected that all mobile device be capable of operating over the entire 700 MHz band. For this purpose small antennas that can be incorporated into handheld devices is of interest. This poses a challenge to design small antennas that can provide the required bandwidth and consistent efficiency over the desired bandwidth. It is also highly desirable to design such antennas planar and for low cost requirement

the antenna structure be compatible with PCB fabrication. Several studies were reported elucidating the relationship between the antenna bandwidth, size and efficiency [29]-[32] and [34].

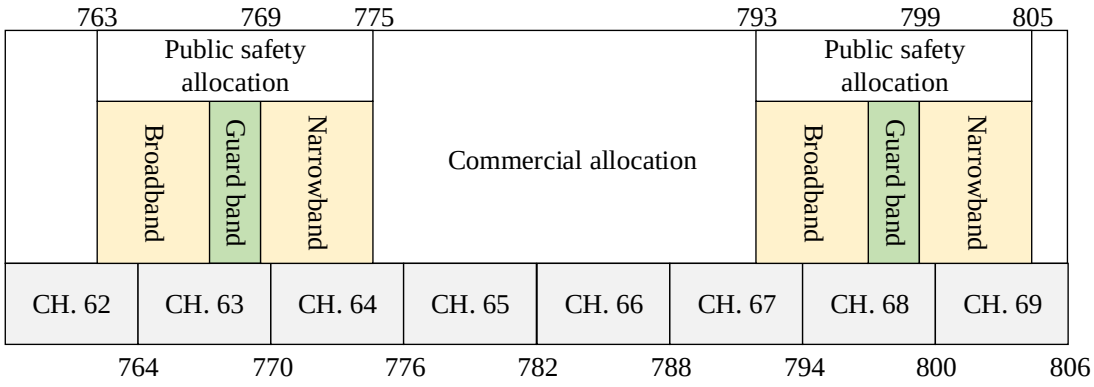

Figure 1.5: The 700 MHz band after enactment of the Spectrum Act.

1.3 Thesis Framework

Chapter 2 introduces a new approach in designing an UWB coupled sectorial loop antenna (CSLA) which is suitable for GPR applications. This antenna has a consistent efficiency and polarization over the band of operation. This new antenna consists of two parallel coupled sectorial loop antennas. A new approach is then presented to make the antenna unidirectional without effecting the antenna's band of operation nor the antenna's dimensions by adding a short cylindrical cavity with a modal suppressing septum. This antenna was fabricated and measured in the Radiation Laboratory at the University of Michigan.

Chapter 3 presents a brief introduction to slot antennas and a new technique to increase the bandwidth of a single slot antenna by creating a fictitious short circuit using an off-centered microstrip feed line. In this chapter, a new approach is used to enhance the bandwidth by using a multi slot elements topology. Each slot element operates in a different bandwidth. Applying the

off-centered feed line methodology on each element will increase the bandwidth significantly. A single microstrip feed line is used to feed all the slot elements.

Chapter 4 introduces a new topology in enhancing a single slot antenna's bandwidth and improving its directivity by combining the slot antenna with a Dielectric Resonance Antenna (DRA). In this chapter, two different superstrate topologies are illusterated to improve the antenna matching with the surroundings especially to the sand. The antenna and two superstrates are then fabricated and measured in the Radiation Laboratory facilities.

Chapter 5 shows a novel miniaturized antenna with omnidirectional horizontally polarized radiation pattern that is suitable for wireless communication applications. The antenna structure resembles a circular loop formed by a circular array of shunt miniaturized n-fold resonant dipole antennas which will be referred to as miniature composite wire-loop antenna (MCWLA). Then, discussing how to feed the antenna and how to eliminate any current excited over the outer layer of the coaxial line used to feed the antenna and finally, antenna fabrication and measurements are presented.

Chapter 6 show a new wideband antenna composed of an array of coupled quarter-wavelength slot antennas that can be used in smartphones for wireless communication applications. This antenna consists of one end open circuited and the other short-circuited is fed by a microstrip feed line and used as the driving element. The resonant frequency is the same as in the $\lambda/2$ slot antenna but the dimension is reduced by half. Using the parasitic coupling effect, a number of $\lambda/4$ slot antennas are positioned around the driving element to achieve the required bandwidth. An advantage of this design is that active circuit components can be place on the top

side of the substrate that supports the microstrip line so long as the slots are not covered or crossed by RF lines.

Chapter 7 concludes this work and illustrates some possible future work related to how to improve the bandwidth and radiation pattern of the designed antennas.

Chapter 2:
Directional Coupled Sectorial Loop Antenna (CSLA)

2.1 Introduction to CSLA

A new type of wide-band antennas is proposed that can provide wider bandwidth and consistent polarization over the operated frequency range while ensuring that the antenna is impedance matched. It consists of two parallel coupled sectorial loop antennas (CSLA) that are connected along an axis of symmetry [35]. Loop antennas have a limited bandwidth because of the large variations in the imaginary part of the input impedance and the large values of the real part of the input impedance at the odd resonance. Dipole antennas have also limited bandwidth because of the large values of the real part of the input impedance at the even resonance and the large variations in the imaginary part of the input impedance. By combining a dipole antenna with loop antenna, great improvement in the matching is obtained. For further improvements, the topology of the loop and dipole antenna is adjusted to have a sectorial loop antenna (SLA). The input impedance, Z_S, of the SLA is a function of three geometrical parameters, R_{out} , R_{in} and α. Such loop antennas, similar to a circular loop, present a parallel-resonance when the antenna circumference is about $C \approx 0.5\lambda$. The equivalent circuit of the antenna is a high-Q parallel *RLC*. This means that it is capacitive above the antiresonance and inductive below the antiresonance. To control the input impedance, two identical antennas can be connected in parallel as shown in Figure 2.1. Therefore, using this new technique controls the coupling between the two antennas. The input

currents are equal but opposite in direction because of the symmetry of the two parallel antennas. This means that the direction of the magnetic field of antenna 1 is opposite to the magnetic field of antenna 2 which yields a strong coupling.

$$V_1 = Z_{11}I_1 + Z_{12}I_2$$
$$V_2 = Z_{21}I_1 + Z_{22}I_2 \qquad (2)$$

Where V and I represent the voltages and currents at the input ports of antennas 1 and 2. Therefore, the input impedance is given as:

$$Z_{in} = \frac{1}{2}(Z_{11} + Z_{12}) \qquad (3)$$

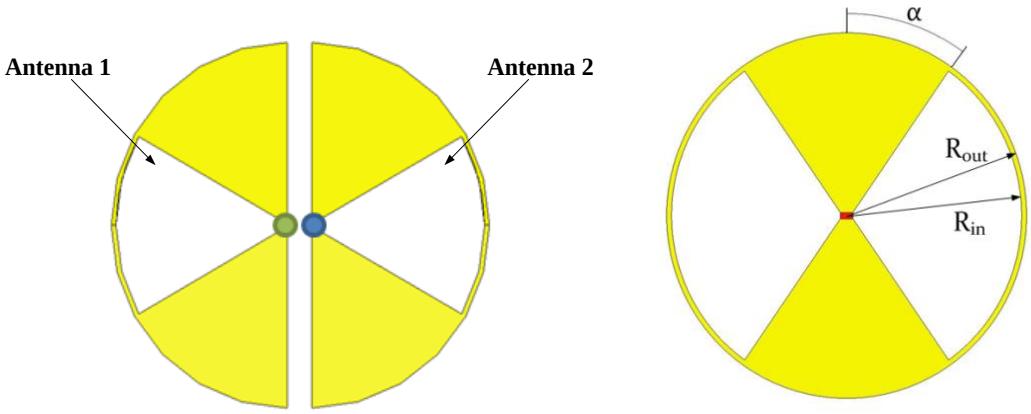

Figure 2.1: Topology of CSLA.

The original three parameters that affect the original CLSA are the inner radius (R_{in}), the outer radius (R_{out}), and the angle α. The following approximate formula determines the lowest operational frequency [35]:

$$f_l = \frac{2c}{(\pi - \alpha + 2)\sqrt{\varepsilon_{eff}}\,(R_{in} + R_{out})} \qquad (4)$$

Inductive loading is used to lower the lowest frequency of operation. It should be emphasized that the radiated field from the slot has the same polarization and maximum direction of radiation as the CSLA. Another important feature of the antenna is its feed. The CSLA is balanced antenna with a plane of symmetry that bisects the loops. As such the input impedance is designed to be around 100Ω. This can be matched to coaxial line using a balun or two 50Ω feed line can be used. Such feed inconjuction with a 180 hybrid can be used to a get an antenna with two input 50Ω input impedance generating the sum and difference radiation patterns. Such antenna can provide radiation pattern diversity that is very useful for UWB communication systems operating in multi-path environment [35]. The effect of the loop angle α can be observed by measuring the current distribution on the CSLA.

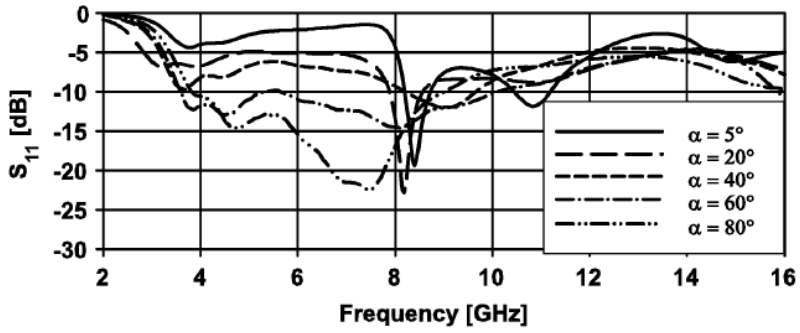

Figure 2.2: Measured S_{11} values for different α values [35].

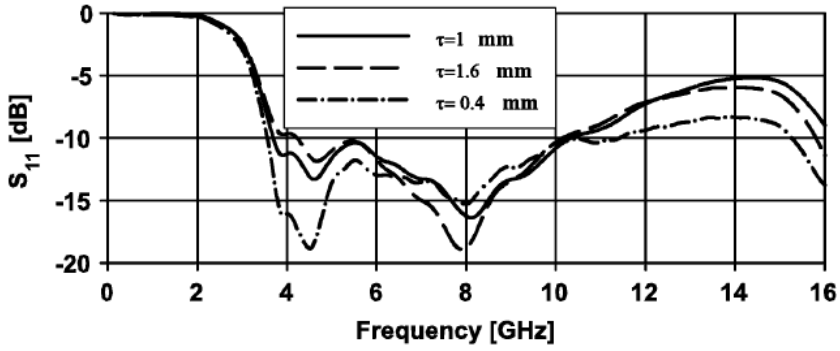

Figure 2.3: Measured S_{11} values for different τ values [35].

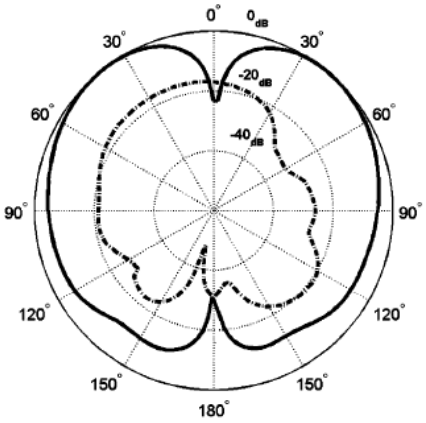

Figure 2.4: Measured radiation pattern of the original CSLA at 2GHz [35].

2.2 Modified CSLA

A number of techniques have been developed in the past to make antennas unidirectional. One of these techniques is placing the antenna in a cavity. For the CSLA, a cylindrical cavity, as shown in Figure 2.5, is used as it is conformal to the CSLA geometry. However, as will be shown, this configuration increases the lowest frequency of operation slightly for the same size CSLA. Another problem in adding the cavity is the generation of in-band cavity resonances the can affect the antenna bandwidth. Many cavity modes can get excited due to the CSLA very wide bandwidth. Due to the size limitation, the diameter of the cylindrical cavity is designed to be the same as the CSLA, which is 100mm. A parametric study is applied to study the effect of the cavity height on the antenna using Ansoft HFSS full wave simulator. For a very short cavity, the metallic bottom wall of the cavity is very close to the CSLA which effects the coupling between the two SLAs. However, increasing the cavity height increases the overall antenna size. Also, the isolation between the two SLA decreases by increasing the cavity height. In addition, for long cavities, the directivity of the antenna is decreased at higher frequencies due to the interference between the antenna direct radiation and the reflected one from the metallic bottom wall. Coaxial cables were

used as the feeding input in order to achieve 50Ω input impedance. As mentioned before, a 180° couple is needed in order to achieve the required input impedance.

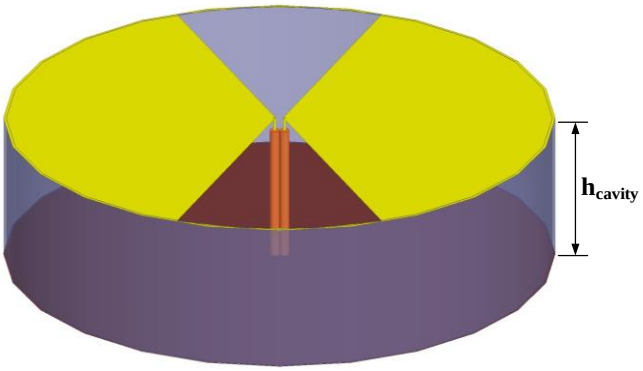

Figure 2.5: CSLA with back cavity.

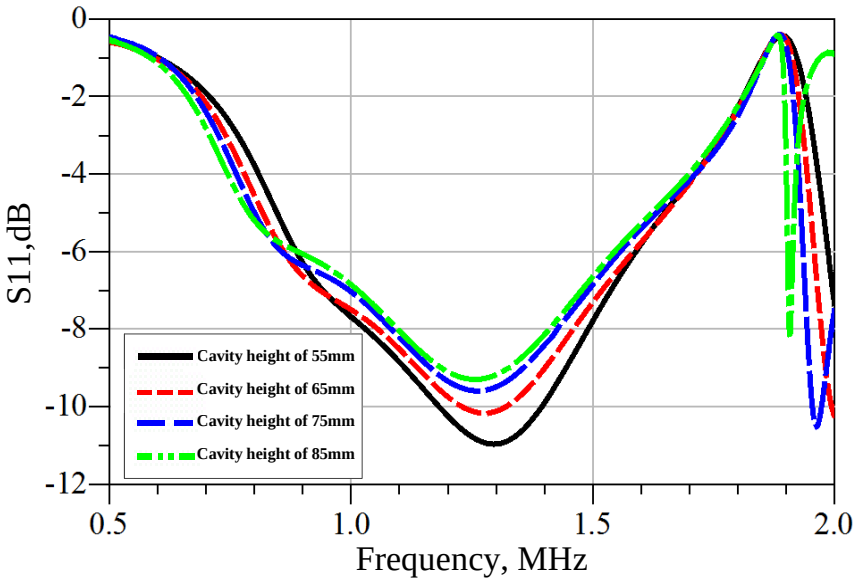

Figure 2.6: The reflection coefficient of the CSLA with back cavity as a function of the cavity height.

The frequency response of the cavity backed CSLA of Figure 2.5 for R_{out}=100mm, R_{in}=99mm, and α=68°, as a function of the cavity height are shown in Figure 2.6. As shown this configuration does not provide the expected bandwidth. To achieve the optimum impedance matching with a small antenna size, h_{cavity}=55mm is chosen. To improve the bandwidth, additional resonances are provided by adding annular slots on the edge of the antenna [36]. Figure 2.7 shows

the geometry of the CSLA with additional pair annular slots encompassing it. The slots become resonant when their arc length is approximately half the wavelength and can help in reducing the lowest frequency of operation.

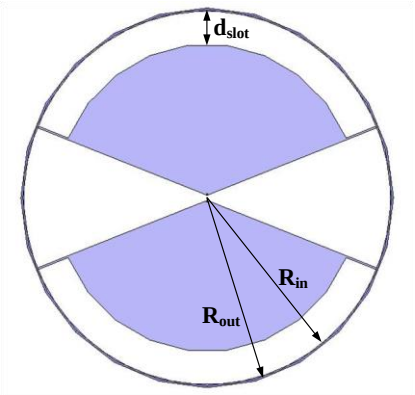

Figure 2.7: CSLA with the annular slot.

By adding the back cavity and the annular slot, the following formula is used to determine the lowest operational frequency [36]:

$$f_{res} \approx \frac{c}{2(R_{out} - \frac{d_{slot}}{2})(\pi - 2\alpha)} \qquad (5)$$

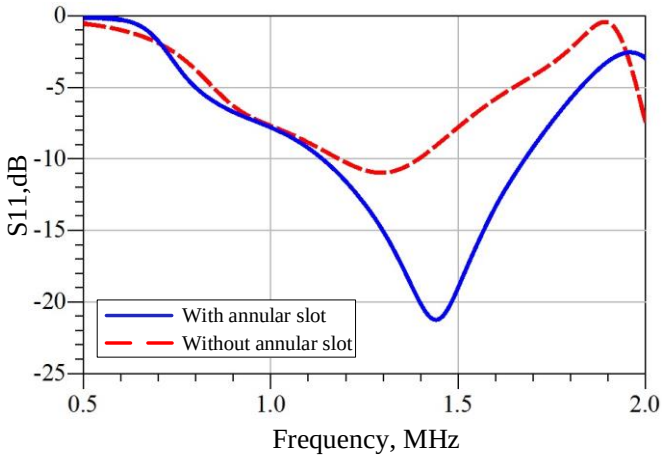

Figure 2.8: The reflection coefficient of the modified CSLA with and without the annular slot.

Figure 2.8 shows how the annular slot improves the bandwidth of the CSLA with back cavity. The CSLA antenna can excite different modes at higher frequencies inside the cavity that can limit the bandwidth of operation. Examination of different cavity modes suggests inclusion of a metallic septum in the cavity in order to suppress some of the cavity modes. The best location for this septum is found to be right under the CSLA wings in a symmetrical fashion. This can be achieved by measuring the field distributions inside the cavity at the frequencies where the reflection coefficients are high. Using Ansoft HFSS full wave simulator, the E-field and H-field distributions can be measured by placing a non-model vertical rectangular and a non-model horizontal circle inside the cavity as can be seen in Figure 2.9. However this septum has to be tapered from edge of the cavity to the center as can be seen in Figure 2.10 so that it would not interfere with the circular magnetic fields that couple the two loops of the CSLA. Additional simulations have been applied to define the tapering angle and the gap in the middle of the septum so it would not interfere the magnetic field of the CSLA.

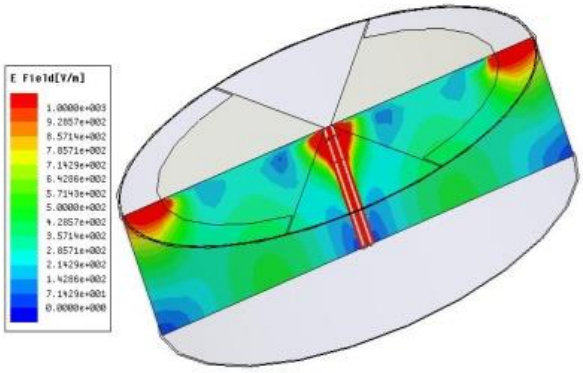

(a)

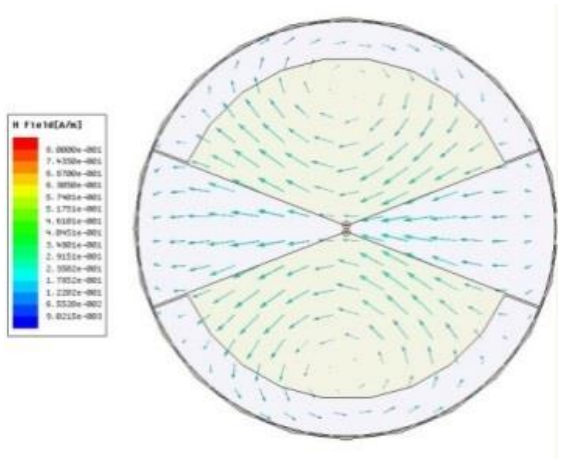

(b)

Figure 2.9: a) The E-field distribution at 2GHz. b) The H-field distribution at 2GHz.

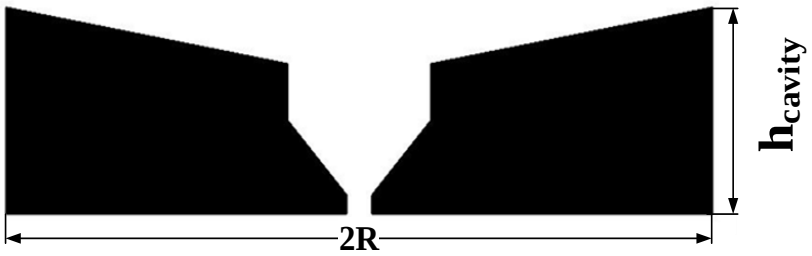

Figure 2.10: The Tapered Fin.

Figure 2.11 shows the location of the tapered fin inside the back cavity of the modified CSLA. Additional simulations have been applied to study the effect of the cavity height on the CSLA with annular slot and the tapered metallic septum (tapered fin). Adding the tapered fin underneath the CSLA improves the reflection coefficient as can be seen in *Figure 2.12*. Figure 2.13 shows that increasing the cavity height decreases the minimum frequency. However, increasing the cavity height increases the antenna overall size by a factor which is higher than the decrease in the minimum frequency. For example, if we increase the cavity height from 55mm to 85mm, the antenna overall size is increased by 54% while the minimum frequency is decreased by 5%. Therefore, the cavity height remains unchanged.

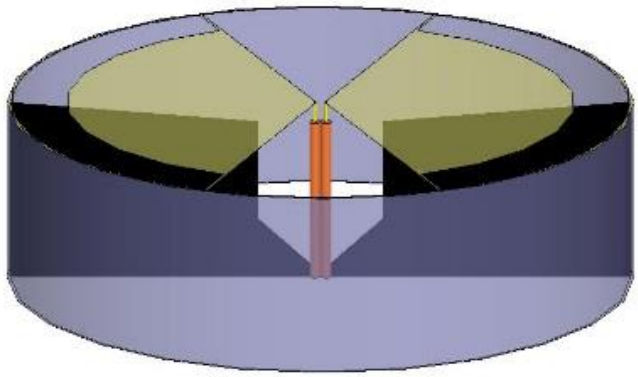

Figure 2.11: CSLA with back cavity and the tapered fin.

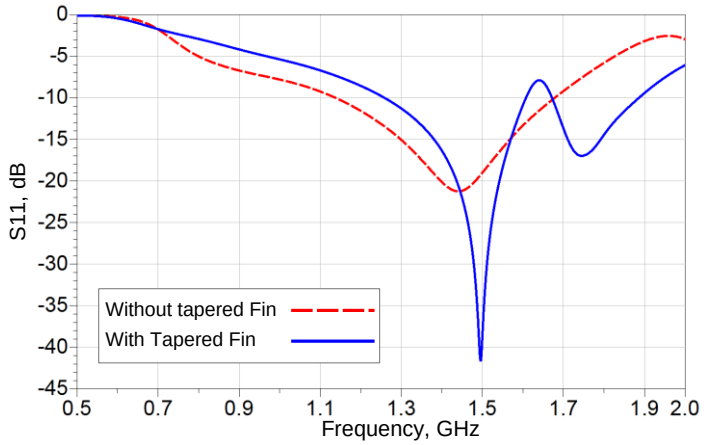

Figure 2.12: The reflection coefficient of the modified CSLA with and without the tapered fin.

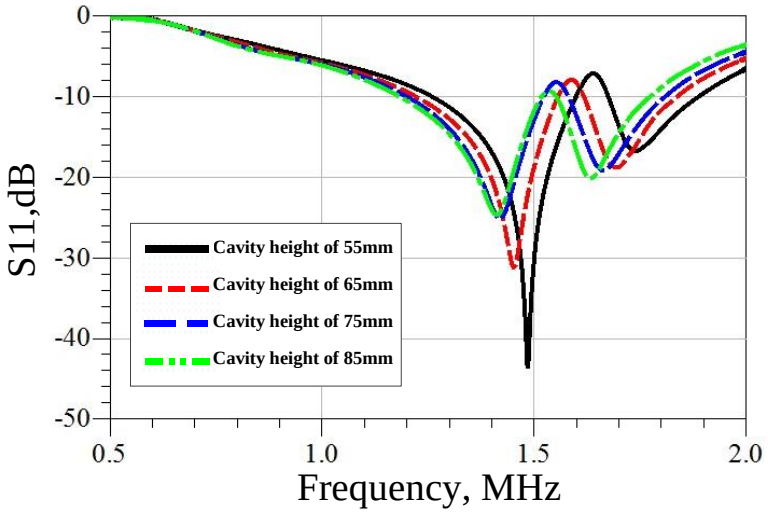

Figure 2.13: The reflection coefficient of the modified CSLA with backed cavity, annular slot, and fin as a function of the cavity height.

To further improve the bandwidth and radiation pattern, a second layer of wings are added over the CSLA with shorting pins on the side (see Figure 2.14). This forms the stacked CSLA geometry that was mentioned earlier. The angle and the height of the upper wings are adjusted by running additional simulations using the Ansoft HFSS simulator to achieve better bandwidth. Figure 2.15 (a) shows the effect of the upper wing on the reflection coefficient and Figure 2.15 (b) shows the radiation pattern of the modified CSLA with the upper annular bowtie. It is noticed that the bandwidth improves by increasing the diameter of the wings but since the size is one of the limiting factors in designing the CSLA, the diameter of the upper wings were chosen to be the same as the diameter of the cylindrical cavity (see Figure 2.16).

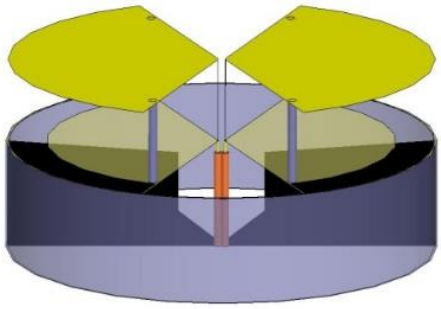

Figure 2.14: CSLA with the second layer of wings.

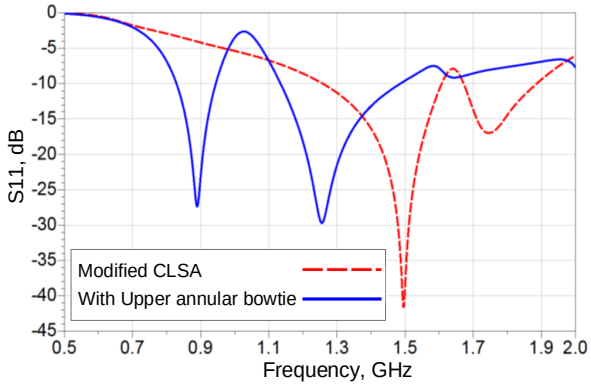

(a)

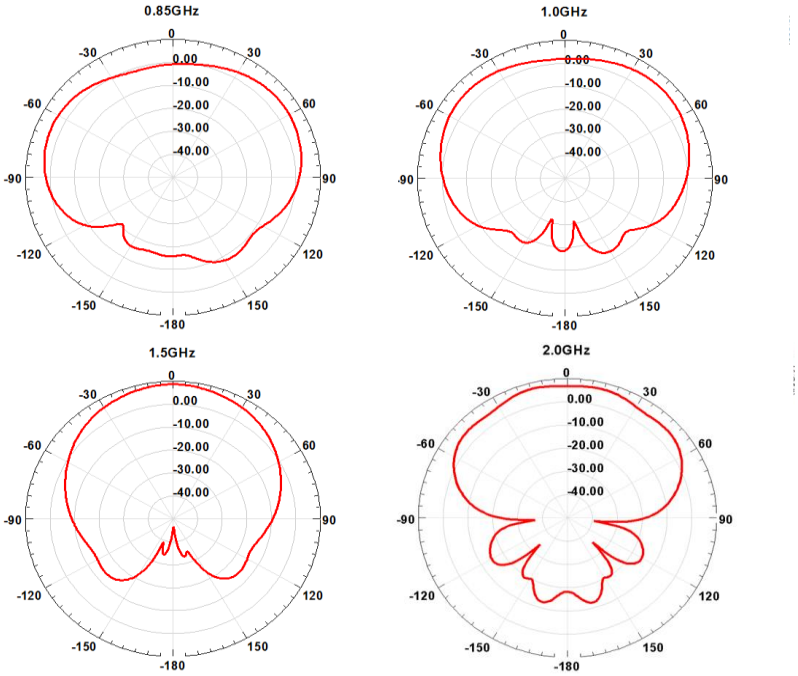

(b)

Figure 2.15: a) The reflection coefficient of the modified CSLA with and without the upper wings. b) The radiation pattern of the modified CSLA with the upper annular bowtie.

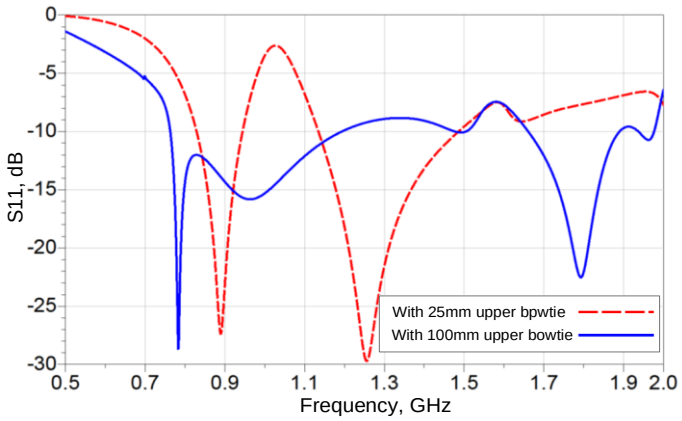

Figure 2.16: The reflection coefficients of the modified CSLA with different upper annular bowtie antenna diameters.

In an attempt to lower the first resonance and improve the Voltage-Standing-Wave-Ratio (VSWR), the length of the slot lines around the edge of the cavity must be increased. But that depends on the optimized angle of the CSLA. An alternative is to create a slow wave slot line. It is noticed that the resonant length of a transmission line can be made smaller if the inductance per

unit length of the line is increased. This can be accomplished by inserting a number of series inductors. Using lumped elements is not possible since they have low Q which affects the antenna efficiency. Instead, narrow short circuited slot-lines can be added along the antenna, [37]. The impedance of the slot lines can be obtained by:

$$Z_S = jZ_{0s}\tan(\beta_g l), \quad (6)$$

where Z_{0s} is the characteristic impedance, l is the length of the slot-line, and β_g is the propagation constant. Inserting short segments of slot-lines on the edge of the antenna effectively increases the length of the slot radiators on the edge without changing the CSLA angle.

The inductive slots are introduces on the both sides to maintain the symmetry of the edge currents. Since the CSLA radial electric currents are near zero at the edge, provision of the inductive slots do not affect the performance of the CSLA. The configuration of the stack CSLA with inductive slots around the edge is shown in Figure 2.17. As can be seen in Figure 2.18, adding the inductive slots will slightly help in improving the bandwidth of the modified CSLA.

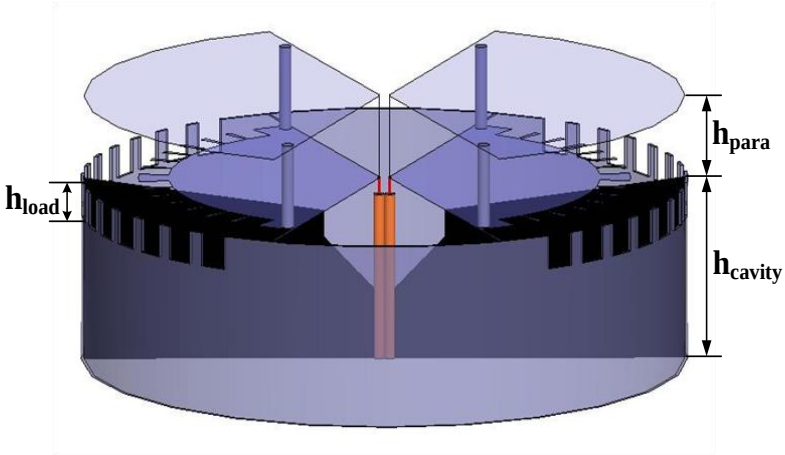

Figure 2.17: The final modified CSLA.

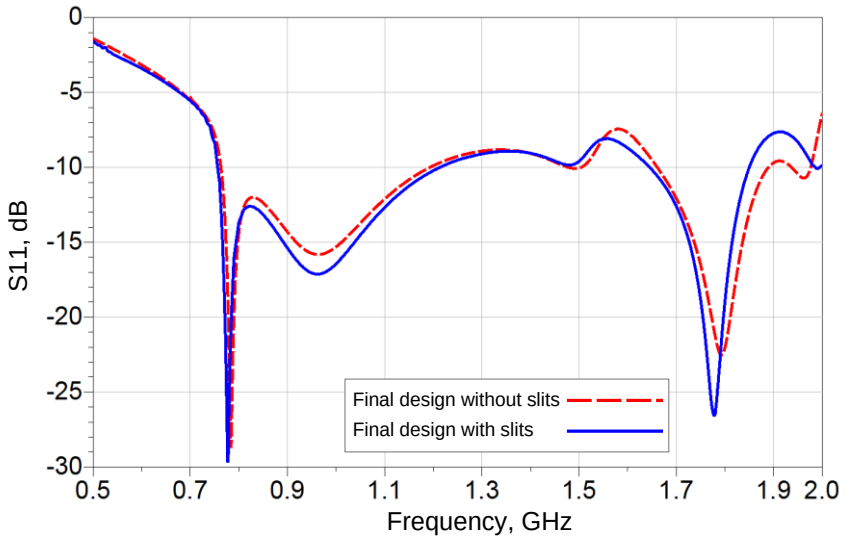

Figure 2.18: The reflection coefficient of the modified CSLA with and without the inductive slots.

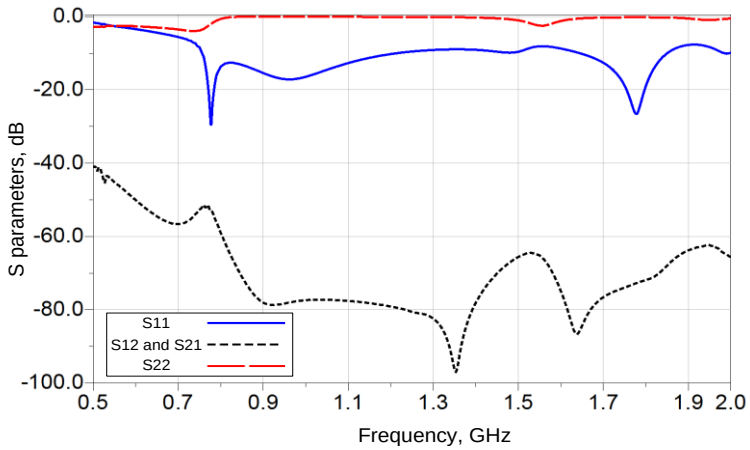

Figure 2.19: Simulated S parameters.

Figure 2.19 shows the S parameters of the final design of the modified CSLA. The final design was fabricated using the following dimensions are used: R_{out} = 100*mm*, h_{cavity} = 55*mm*, h_{para} = 25*mm*, h_{load} = 10*mm*, w_{slot} = 18*mm*, and $\alpha = 22^{o}$.

2.3 Measurements and results

Figure 2.20 shows the final design prototype. The antenna, the parasitic and the fin were fabricated using Rogers RO4003C substrate of 60mil (1.524mm) thickness and dielectric constant of 3.38. Rogers 3003 of 5mil (0.13mm) thickness and dielectric constant of 3.00 was used in

fabricating the cylindrical cavity. The fabricated antenna has a diameter of 100mm and a height of 80mm. The reflection coefficient of the fabricated antenna was then measured using two 50Ω feed lines in conjunction with a 180 hybrid and connected to a calibrated HP8720D vector network analyzer. Figure *2.22* shows the measured and simulated VSWR. The figure shows that the antenna has a bandwidth of 38%. It is noticeable that the measured result is in a good agreement with the simulation. However, the deviation can be attributed to the fabrication process.

Figure 2.20: The prototype of the directional CSLA.

Figure 2.21: The 180^{o} coupler used in measuring the fabricated CSLA.

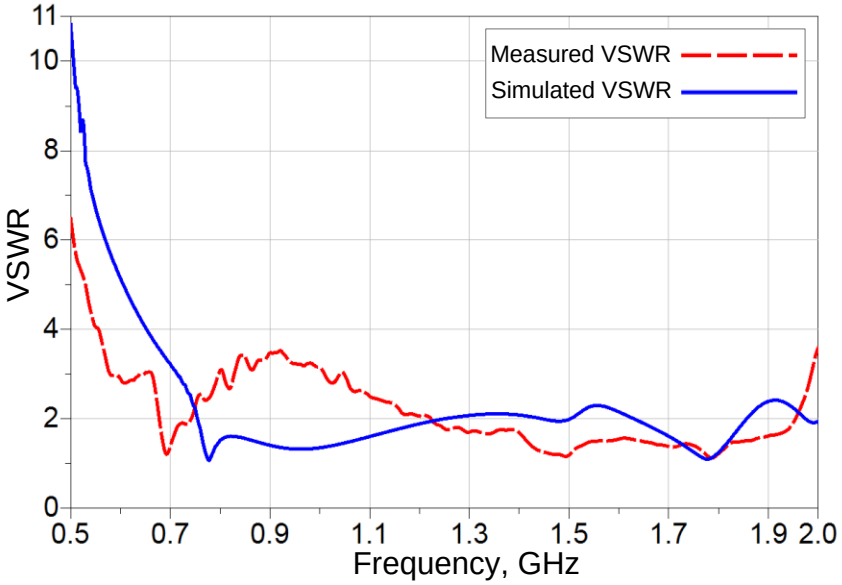

Figure 2.22: Measured and simulated VSWR of the final modified CSLA.

Chapter 3:
Different broadband slot antenna designs

3.1 Background

One of the most popular planar low-profile antennas is the slot antenna. Slot antennas have been investigated widely in the last few decades as they are easy to fabricate, are easy to integrate with active devices, have high radiation efficiencies, and are low-cost [38]-[40]. They are very suited for communication due to their almost omnidirectional radiation pattern. At the first resonant frequency, a slot antenna has a length of about $\lambda g/2$ where λg is the guided wavelength influenced by the substrate dielectric constant and thickness. The bandwidth of slot antennas is proportional to the area of open aperture. Although the width of the slot antenna is very small ($w << \lambda g$), the currents are not limited to the edges of the slot but spread out over the sheet. Slot antennas behave according to Babinet's Principle which is stated as follows:

The field at any point behind a plane having a screen, if added to the field at the same point when the complementary screen is substituted, is equal to the field when no screen is present

This principle however doesn't consider polarization. Babinet's principle has been extended and generalized by Booker [41] to take into account the vector nature of the electromagnetic field. It assumed that the screen is a perfectly conducted and very thin plane. The polarization of a slot antenna is linear. The radiation pattern of the slot antenna is the same as a $\lambda/2$ dipole antenna with two differences: 1) The E- and H-fields are interchanged and 2) The

component of the electric field of the slot normal to the plane is discontinuous from one side of the plane to the other.

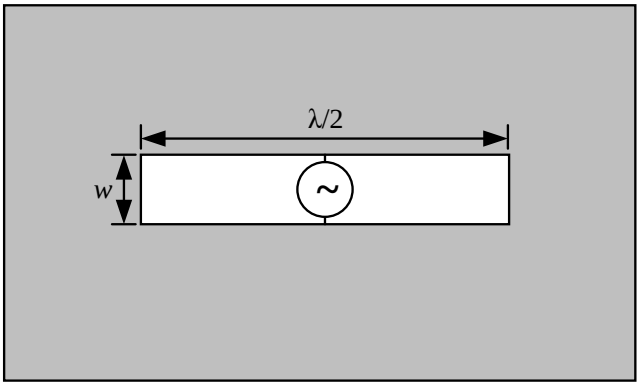

Figure 3.1: λ/2 Slot antenna

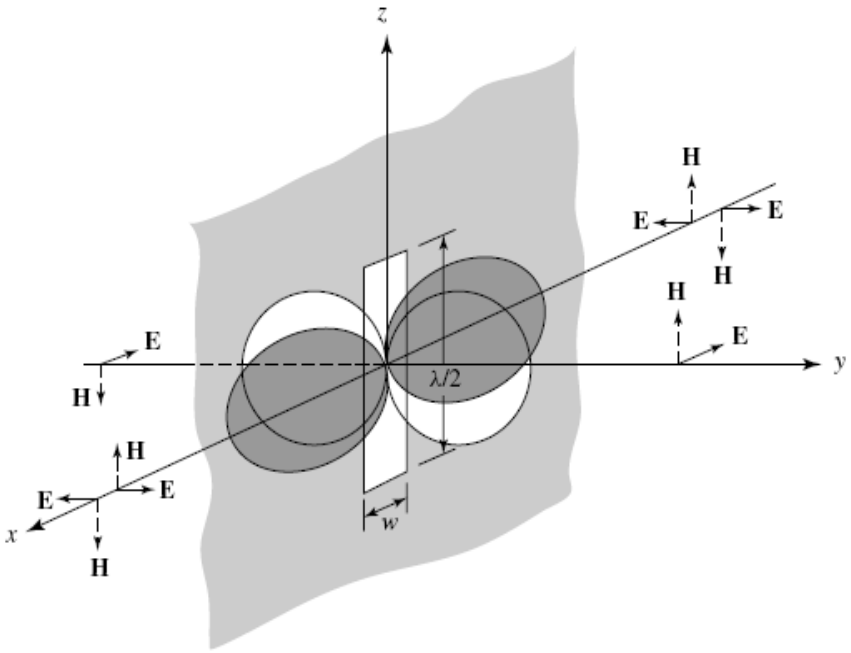

Figure 3.2: Radiation pattern of $\lambda/2$ slot antenna [42].

Since the slot antenna is in a vertical position as in Figure 3.2, the antenna radiation is then horizontally polarized. The E-field has only E_ϕ component. If the slot antenna is λ/2 long and width is very small ($w << \lambda$), then E_ϕ is given by:

$$E_{\phi} = \frac{\cos[(\pi/2)\cos\theta]}{\sin\theta} \qquad (7)$$

The impedance of the slot antenna, Z_s, is related to the impedance of its complementary dipole antenna, Z_d, by the following relation:

$$Z_d Z_s = \frac{\eta^2}{4} \qquad (8)$$

Where η is the intrinsic impedance of free space.

3.1.1 Off-centered Microstrip-fed Slot Antenna

One way to increase the bandwidth of a single slot antenna is to create multiple resonant conditions within the antenna structure. However, a dual-band slot antenna was studied and presented in 2005 [43] where it shows that, an off-centered, microstrip fed, slot antenna with a proper design can create a fictitious short circuit near the microstrip feed. This fictitious short circuit produces a second resonance at a frequency slightly above the first resonance which produces the dual-resonant behavior.

Placing the microstrip feed near to an edge, produces an electric field in the opposite direction of the electric field in the slot and hence by proper design a null filed in the slot line (fictitious short) corresponding to a second resonance will be produced. Basically the electric field of the slot antenna excited by the return current on the ground plane is canceled out by the tangential electric field created by the narrow microstrip feed line [43]. Figure 3.3 shows the topology of the off-centered microstrip-fed slot antenna.

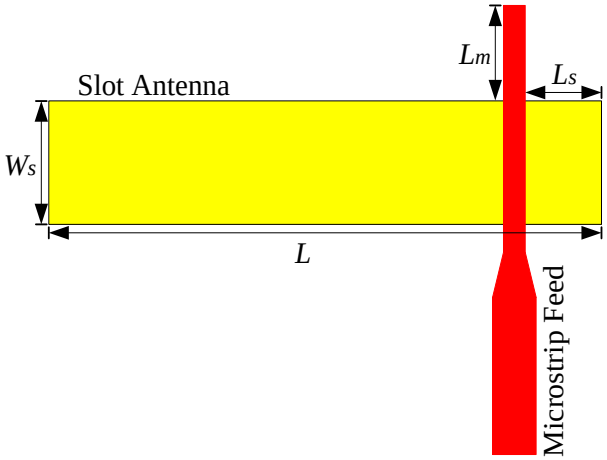

Figure 3.3: Off-centered microstrip-fed Slot Antenna.

The parameters that affect the existence and the location of the fictitious short circuit are:

(a) The width of the slot antenna.

(b) The width of the microstrip antenna.

(c) The distance between the microstrip line feed and the edge of the slot antenna.

It is noticed that, the second resonant frequency increases by increasing the distance between the microstrip line feed and the edge of the slot antenna, L_s. Therefore, choosing the proper distance, L_s, the total bandwidth increases and a dual-band operation is achieved. Optimizing the length of the open circuit microstrip feed line, L_m, improves the matching. Figure 3.4 shows the reflection coefficient of the off-centered microstrip-fed slot antenna. The slot antenna length (L) is approximately $\lambda_g/2$ at the first resonance (L = 400 mm), where λ_g is the wavelength in the slot line forming the antenna. The width of the slot antenna (W_s = 50 mm) is kept much smaller than the wavelength. The length and width of the slot antenna are then adjusted to achieve the desired dual band.

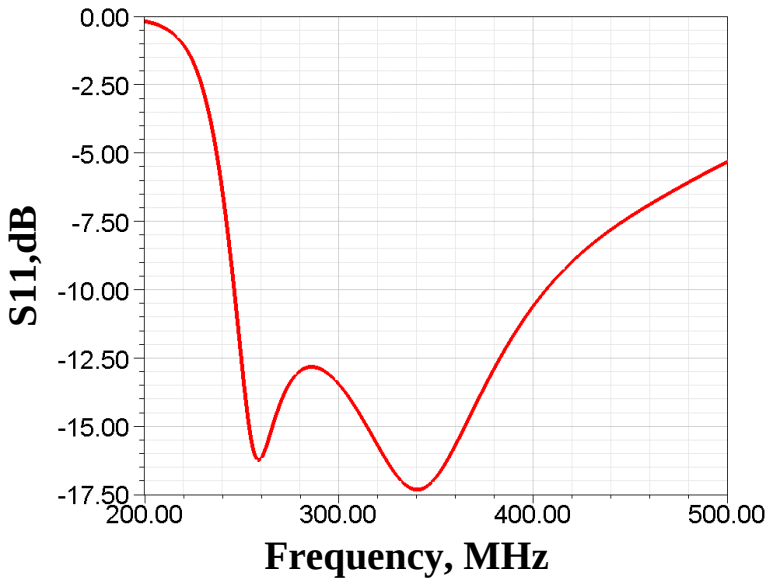

Figure 3.4: The reflection coefficient of the off-centered microstrip-fed slot antenna with L = 400mm, W_s = 50mm, L_s = 90mm, L_m = 35mm on a substrate with thickness of 0.5mm and dielectric constant of 2.2.

3.2 Quadruple-Element Slot Antenna

3.2.1 Antenna Design

It is expected that designing antenna that is composed of two or more radiators can present very wide-band characteristics. [43] shows that the bandwidth of a slot antenna can be enhanced by adding a second slot element. There are a number of different multi-element feeding topologies, in which a single feeding element can be used. These topologies include:

(a) Feeding in Series

(b) Feeding in Parallel

(c) Feeding through Parasitic coupling

It was observed that the wide-band behavior can be achieved when the antenna is fed directly with a microstrip line. Therefore, parasitic coupling is not the right alternative to use in order to provide the best results. Using a single microstrip line to feed the two elements in a series fashion

is a possible choice and it is commonly used in end fire arrays antennas. [43] shows that the parallel feed topology is a great alternative for multi-element antenna since it provides better flexibility in designing the feeding network and designing a broadside radiation pattern antenna. It also makes the antenna impedance matching easier to be achieved.

In this design, a new technique is presented to further improve the bandwidth. Adding two additional slot elements with chosen lower and upper operating frequencies will improve the bandwidth without significantly increasing the size of the antenna. Each slot element is chosen such that all the four slot elements will cover a very wide-band. Each set of two elements are fed with two microstrip lines connected in parallel. Then they are all connected to a single microstrip line feed. As a result, a quadruple-element slot antenna is achieved. The first two slot elements, the lower operating frequencies part, operate from 0.9GHz to 2.2GHz. The first element operates from 0.9GHz to 1.4GHz while the second one operates from 1.4GHz to 2.2GHz. Each element is fed with a single microstrip line. The off-centered microstrip-feed line technique is used on each slot element to achieve the desired bandwidth. These microstrip lines are connected in parallel to have a single feed that feeds both elements. The microstrip feed network was modified to achieve the desired response. Figure 3.5, (a) shows the double-element slot antenna design with a parallel feed topology and (b) shows how the bandwidth of the double-element slot antenna has improved.

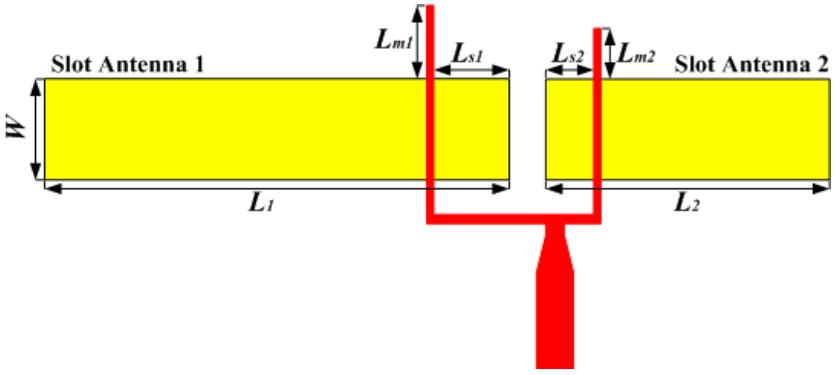

(a)

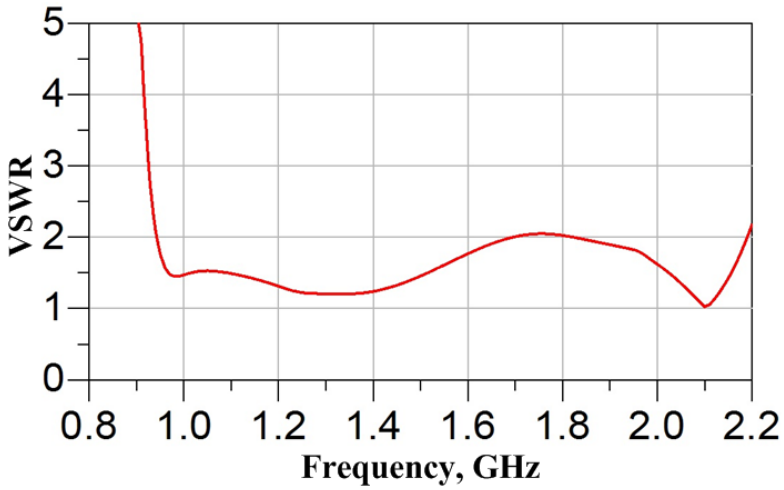

(b)

Figure 3.5: a) Double-element slot antenna and b) The VSWR of the double-element slot antenna.

Similar to the first two slot elements set, the second two elements set (the higher operating frequencies part) is designed. These two additional elements combined operate from 2.2GHz to 6GHz. Using the Ansoft HFSS simulator, the width and length of each element are chosen to achieve the desired operating bandwidth (see Figure 3.7). However, feeding all the four elements with a single microstrip feed line won't give the desired response due to the impedance mismatch between the high and low frequencies (see Figure 3.7).

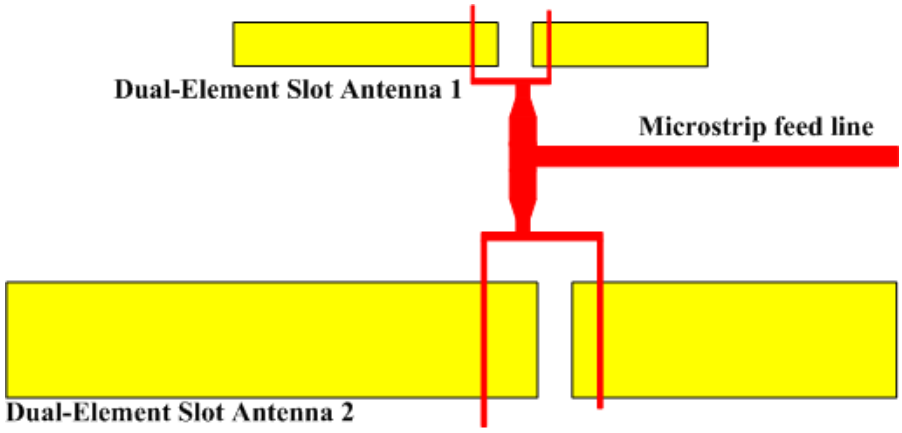

Figure 3.6: Quadruple-element slot antenna topology and

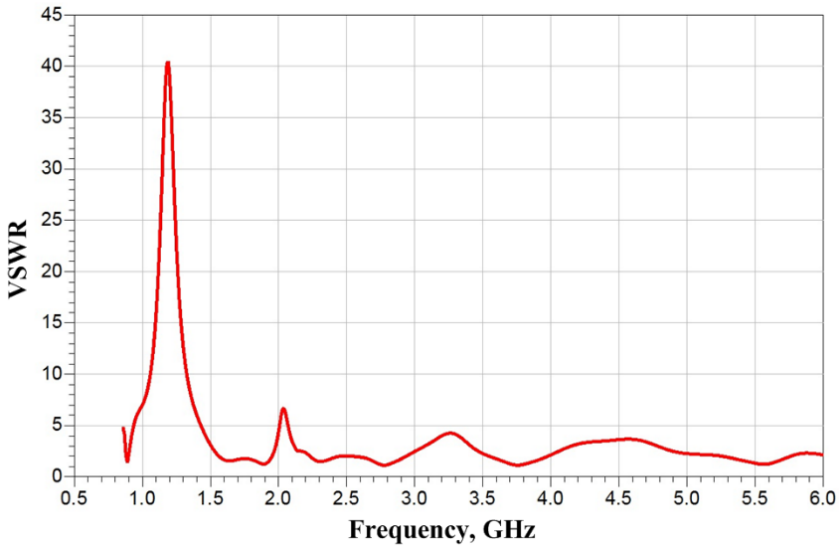

Figure 3.7: VSWR of the quadruple-element slot antenna.

In order to achieve better bandwidth behavior, low- and high-pass matching networks were added to the feeding network to improve the matching. The length and width of the microstrip feed were optimized using the ADS simulator to match to 50Ω. Figure 3.8 shows the final design of the quadruple-element slot antenna using the low and high pass matching networks to feed each element with a microstip lines in a parallel fashion.

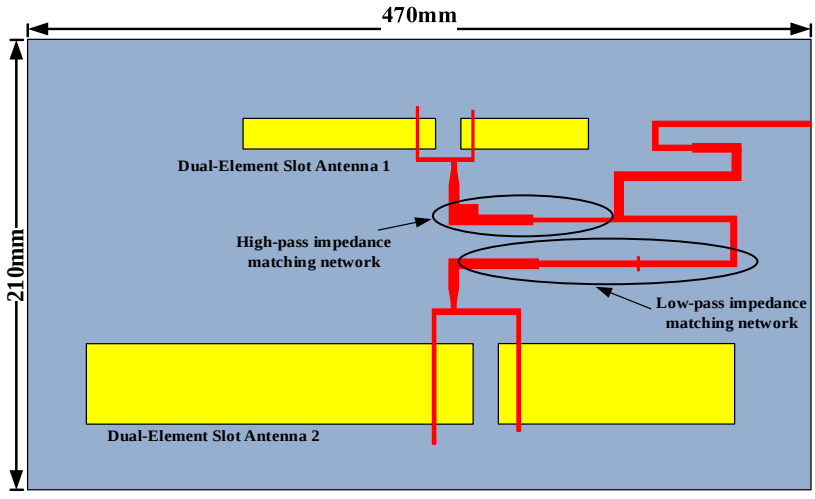

Figure 3.8: Quadruple-element slot antenna final design with the matching network.

3.2.2 Measurements and results

The quadruple-element slot antenna was fabricated using Rogers RO4350 substrate of 0.5*mm* thickness and dielectric constant of 3.4. The antenna was then connected to a calibrated HP8720D vector network analyzer to measure the VSWR. Figure 3.9 shows the measured and simulated VSWR. It is noticeable that the measured result is in a good agreement with the simulation. However, the deviation can be attributed to the fabrication process. Figure 3.10 shows the measured E- and H-plane radiation pattern using the anechoic chamber in the radiation laboratory.

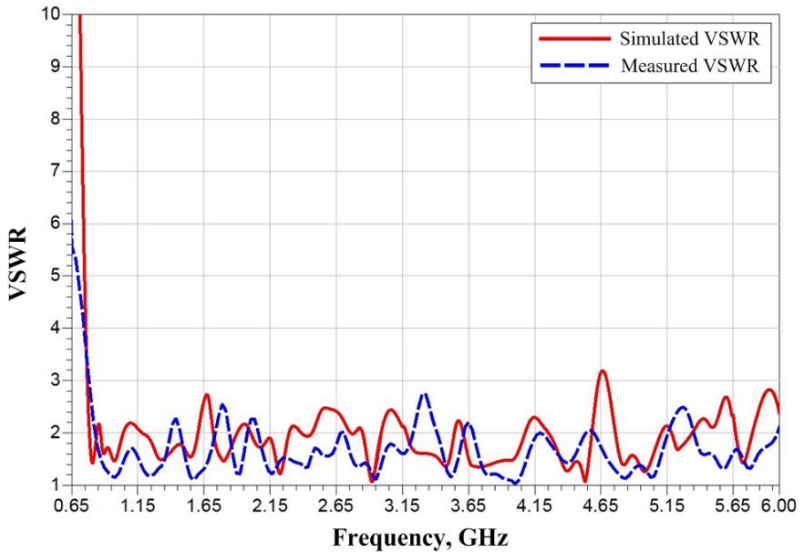

Figure 3.9: Measured and simulated VSWR of the quadruple-element slot antenna final design.

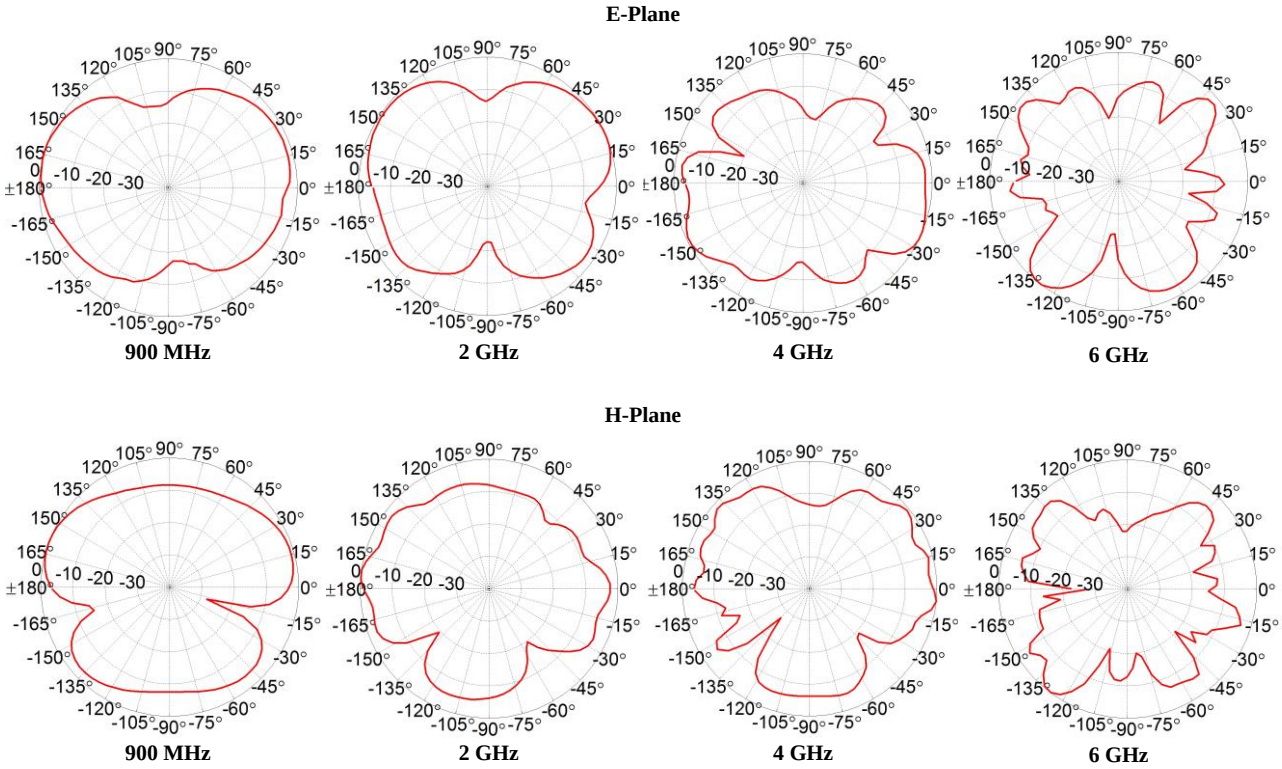

Figure 3.10: The E- and H-planes radiation patterns for different frequencies.

Chapter 4:
Slot Antenna with Graded Index Superstrate

4.1 Approach I

4.1.1 Graded Index Superstrate Design

In addition to the off-centered, microstrip fed, slot antenna that creates a fictitious short circuit near the microstrip feed which produces a second resonance at a frequency slightly above the first resonance, another technique used to improve the bandwidth is to combine the slot antenna with a Dielectric Resonance Antenna (DRA). Dielectric resonance antennas are widely used in different antenna applications due to its low cost, wide band and high efficiency and inherently wide bandwidth [44]-[48]. Their designing process is flexible and are easy to integrate into any fabrication technology. It was observed that with proper design of the slot antenna and the DRA, a dual-band operation can be achieved by merging the two resonances of the slot antenna and the DRA. In order to further improve the bandwidth, a number of parasitic elements can also be added. Placement coplanar parasitic slot elements close to the slot antenna creates strong coupling among them which can lead to wideband operation [49] and [50] .

It has been reported that adding a superstrate over a slot antenna can be used to reduce the antenna size and improve the antenna front-to-back ratio [51][52]. However, use of superstrtae for reducing the size of the slot antenna comes at the expense of narrower bandwidth. However, it has been shown that dimensions and dielectric constant of a finite superstrate can be designed in such

a way to excite a dielectric resonator mode that can easily be merged with that of the exciting slot antenna to achieve a dual mode operation [44]. To lower the quality factor of the dielectric resonator and achieve a higher bandwidth use of magneto-dielectric materials with permittivity almost equal to permeability was proposed in [53]. Such materials with low index contrast tend to present higher bandwidth. The drawback is the magnetic loss factor of the material that tends to lower the antenna efficiency at upper VHF and UHF bands. An alternative is to use graded index lens with high dielectric constant in contact with the slot antenna and lower dielectric near the top. The high dielectric in contact with the slot antenna can reduce the size of the slot antenna significantly and thus the slot antenna can only radiate effectively towards the superstrate direction leading to significant reduction in the backward radiation. It should however be noted that the backward radiation is also a function of the slot antenna ground plane size compared to the wavelength. The graded index allows a better matching to free-space and reduces the quality factor of the dielectric resonator.

Due to the limitation of material availability, two different low-loss materials (glass and polycarbonate) are used as a stepped index superstrate. The dielectric constant of the glass and the polycarbonate used for the antenna design are measured to be 7.2 and 4 respectively. The thicknesses of both the glass and the polycarbonate layers are chosen according the material availability in the Radiation Laboratory to achieve the desired antenna response.

Figure 4.1 (b) shows the side view of the slot antenna substrate with the glass and the polycarbonate superstrates and Figure 4.2 shows the perspective view of the slot antenna with the stepped index superstrate.

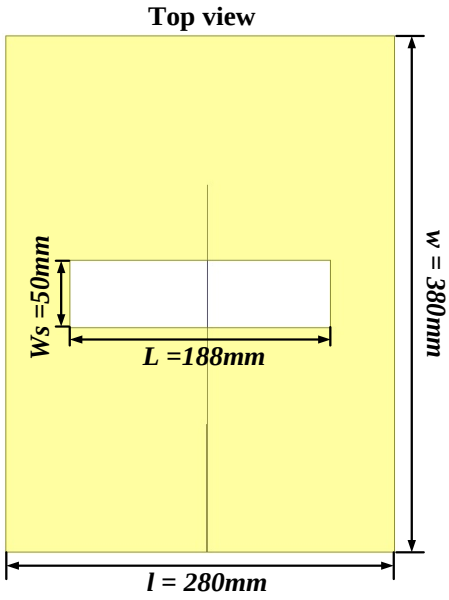

(a)

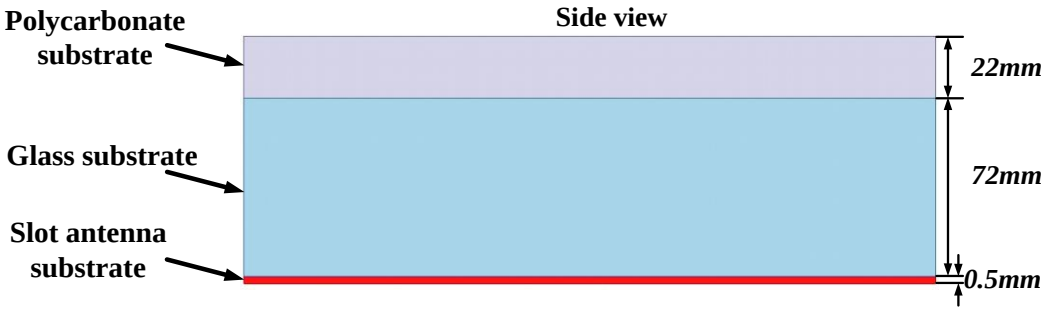

(b)

Figure 4.1: a) The top view of the slot antenna. b) The side view of the slot antenna substrate and the graded index superstrate with dimensions.

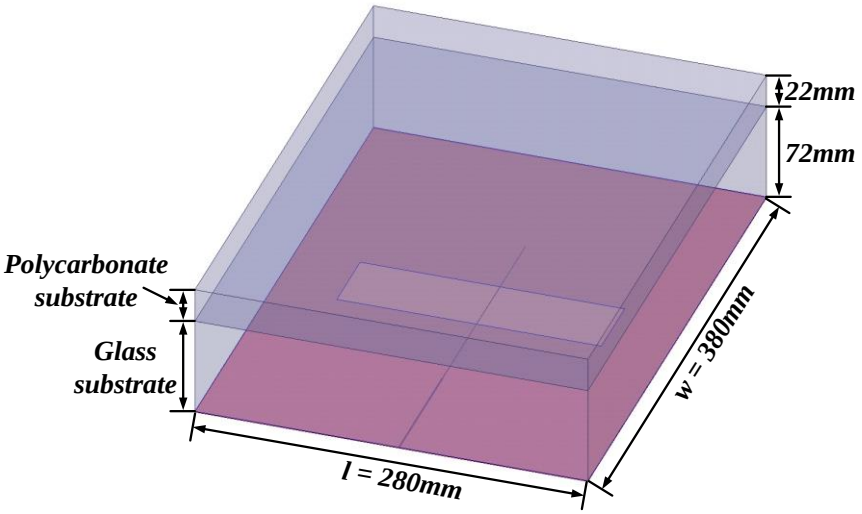

Figure 4.2: Slot antenna with a steppeded index superstrate.

It was observed that adding the graded index superstrates on top of the slot antenna shifts the resonances to a lower frequency range since the size of the overall antenna is considered to be increased. The feed line is designed to improve the matching to 50Ω microstrip line.

The frequency responses of the antenna return loss are shown in Figure 4.3 as the length of the slot antenna , *L*, is varied from 188 mm to 208 mm with 10 mm increment while the width remains the same, *Ws* = 50 mm. In Figure 4.4, the dimensions of the superstrate are varied. The nominal dimensions are: Length, *l* = 280 mm and the width, *w* = 380 mm. The dimensions of the slot antenna remain the same. In Figure 4.4, (a) shows the reflection coefficient of the slot antenna with the superstrate with the nominal dimensions of the superstrate, (b) shows the S_{11} when the width is reduced to *w* = 411 mm and the length, *l* was kept the same, (c) shows the S_{11} when the length is *l* = 309 mm and the width, was kept at *w* = 380 mm, and (d) shows the S_{11} when the length is *l* = 309 mm and the width is *w* = 411 mm. It is concluded that the upper resonance is affected by the superstrate dimensions.

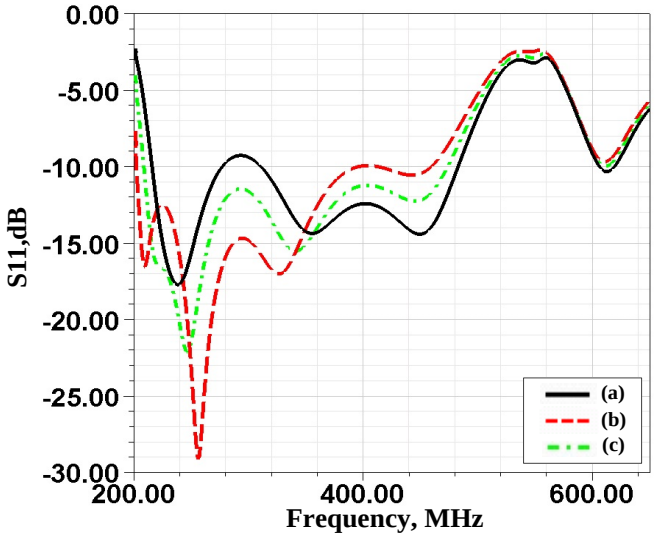

Figure 4.3: The reflection coefficient of the slot antenna with graded index superstrates. Length of the slot antenna is varied. (a) the original length L = 188 mm. (b) L = 208 mm. (c) L = 198 mm.

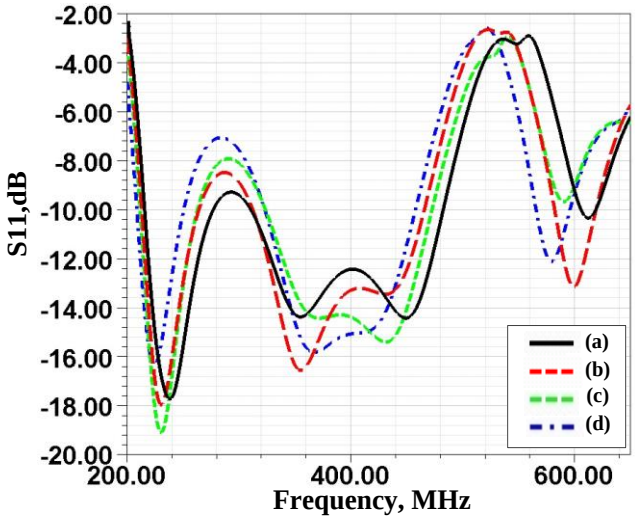

Figure 4.4: Length l and width w of the superstrate are varied. (a) Original dimensions, l = 280 mm, w = 380 mm. (b) l = 280 mm, w = 411 mm. (c) l = 309 mm, w = 380 mm. (d) l = 309 mm, w = 411 mm.

4.1.2 Parasitic Elements Effect

So far it was demonstrated that using a wide slot antenna assisted by a fictitious short and suprestrate DRA can enhance the bandwidth. Another technique to further enhance the antenna bandwidth is to add parasitic elements. This technique has become more popular for its ability to

improve the fundamental characteristics of an antenna such as polarization, gain, input impedance and radiation pattern [54] and [55].

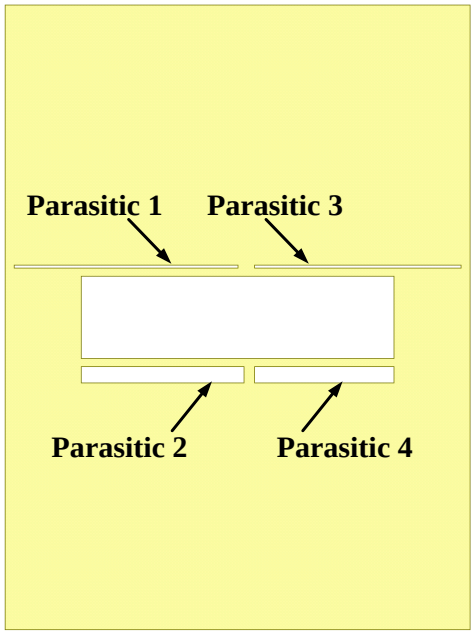

Figure 4.5: Top view of the slot antenna showing the four parasitic elements.

Figure 4.5 shows the slot antenna with four different possible parasitic elements around the slot antenna to increase the bandwidth at higher frequency band of operation. Placing the four parasitic elements close enough to the slot antenna creates strong coupling between the slot antenna and the parasitic elements. The location and dimensions of the four parasitic elements are chosen by trial and error method, using the Ansoft HFSS full wave simulator.

Comparison between the reflection coefficients of the slot antenna with the stepped index superstrate and the inclusion of only one parasitic element at a time are shown in Figure 4.6. Figure 4.7 shows the reflection coefficients of the slot antenna with increasing inclusion of the parasitic elements.

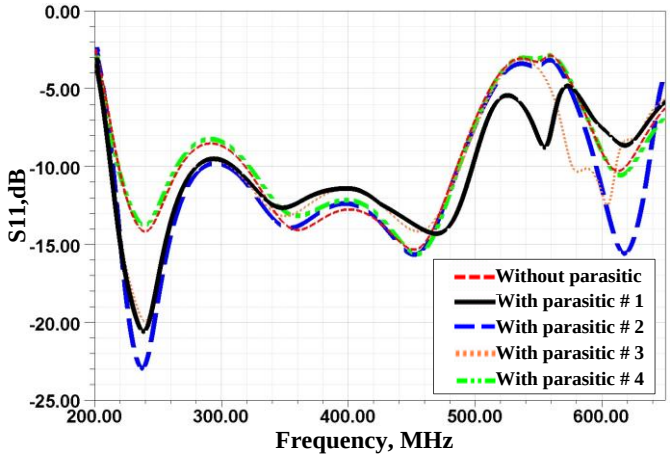

Figure 4.6: Comparison between the reflection coefficients of the slot antenna with each parasitic and without any parasitic.

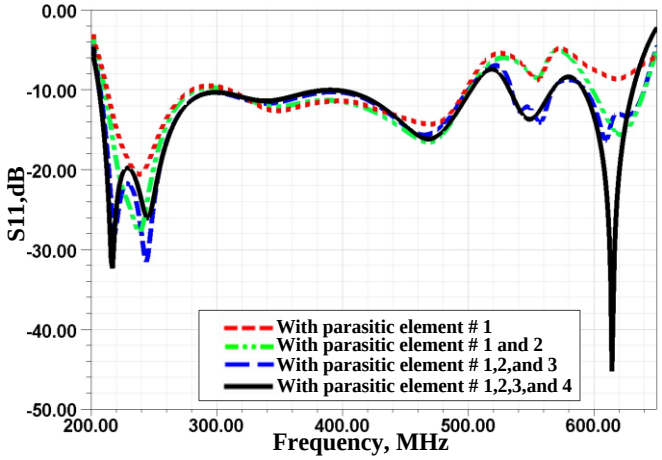

Figure 4.7: Comparison between the reflection coefficients of the slot antenna with 1,2,3 and 4 parasitic elements.

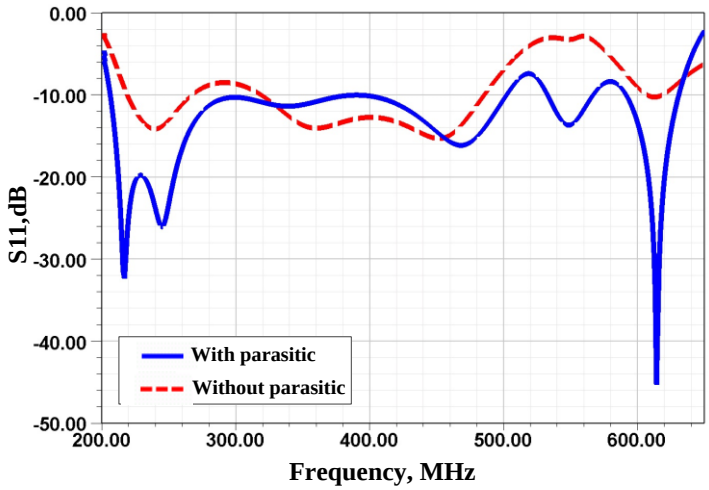

Figure 4.8: The reflection coefficient of the slot antenna with graded index superstrate without the parasitic elements and with four parasitic elements.

Figure 4.8 shows a comparison between the reflection coefficient of the slot antenna with the stepped index superstrate with and without the four parasitic elements. It was noticed that the reflection coefficient improves by adding the four parasitic elements around the slot antenna. The final design of the slot antenna is then fabricated.

4.1.3 Measurements and Results

The prototype was fabricated on a Rogers RT/Duroid 5880 substrate with dielectric constant of 2.2 and 0.5mm thickness using the standard PCB technology. Glass and polycarbonate are used to assemble the graded index superstrates with tapered dielectric. The dielectric constant of the glass and the polycarbonate were measured to be 7.2 and 4 respectively. The thickness of the glass is 72mm and the thickness of the polycarbonate is 22mm. The dimensions of the antenna are 380mm x 280mm x 94mm. Four parasitic elements were added to improve the bandwidth. The dimensions of the parasitic elements were modified to achieve the required response. The superstrate, which consists of the glass and polycarbonate, is placed on top of the slot antenna as shown in Figure 4.13. The reflection coefficient is then measured using a vector network analyzer. It shows that the antenna has a bandwidth of 35.5%. The measured reflection coefficient is compared with the simulate results as shown in Figure 4.9 where a good agreement between the simulation and measured results is observed. The deviation can be attributed to the fabrication process. An important feature of the wideband antenna is its gain and radiation pattern. Figure 4.10 shows the simulated and measured gain of the slot antenna. The gain was measured inside the anechoic chamber of the Radiation Laboratory at the University of Michigan. As can be seen in Figure 4.11, the electric field is concentrated in the upper half space which indicates that the radiation is taking place in the front side of the antenna. The back ratio is mainly due to finite size of the ground plane which is higher at lower frequencies.

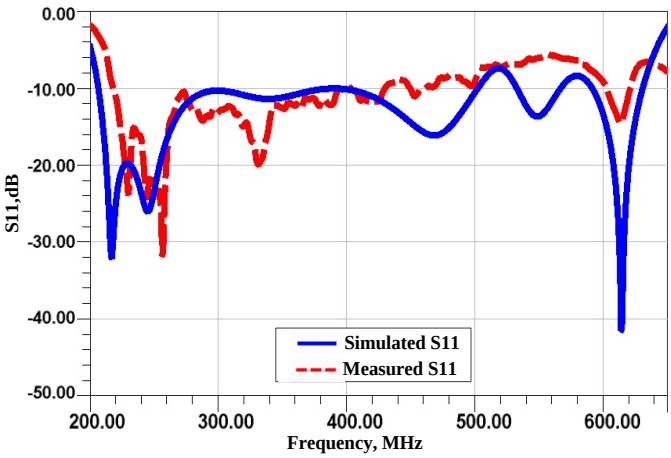

Figure 4.9: The measured and simulated reflection coefficient of the slot antenna with graded index and four parasitic elements.

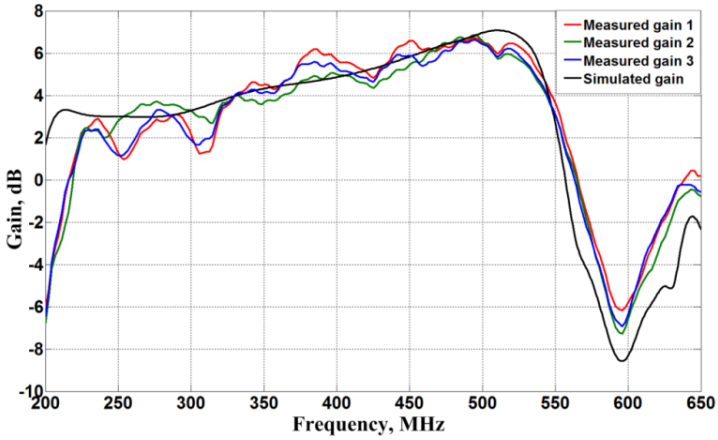

Figure 4.10: The simulated and measured gain.

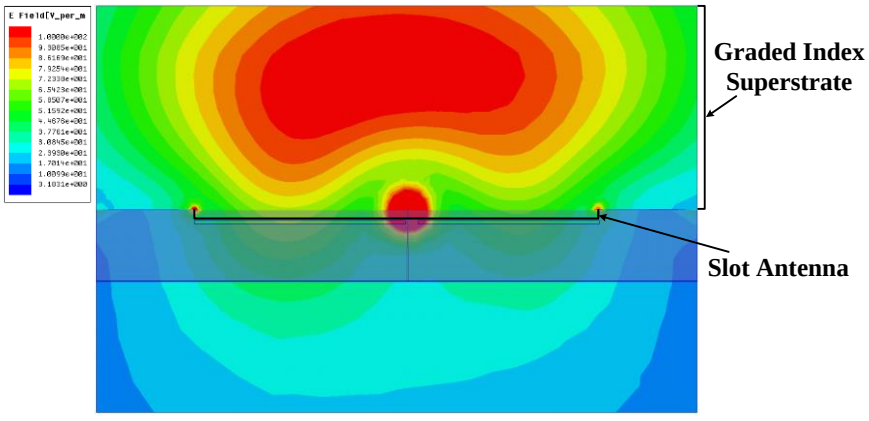

Figure 4.11: The electric field distribution of the slot antenna with graded index supserstrate and four parasitic elements at 400MHz. The concentration of fields in the superstrate indicates the directional radiation of the antenna.

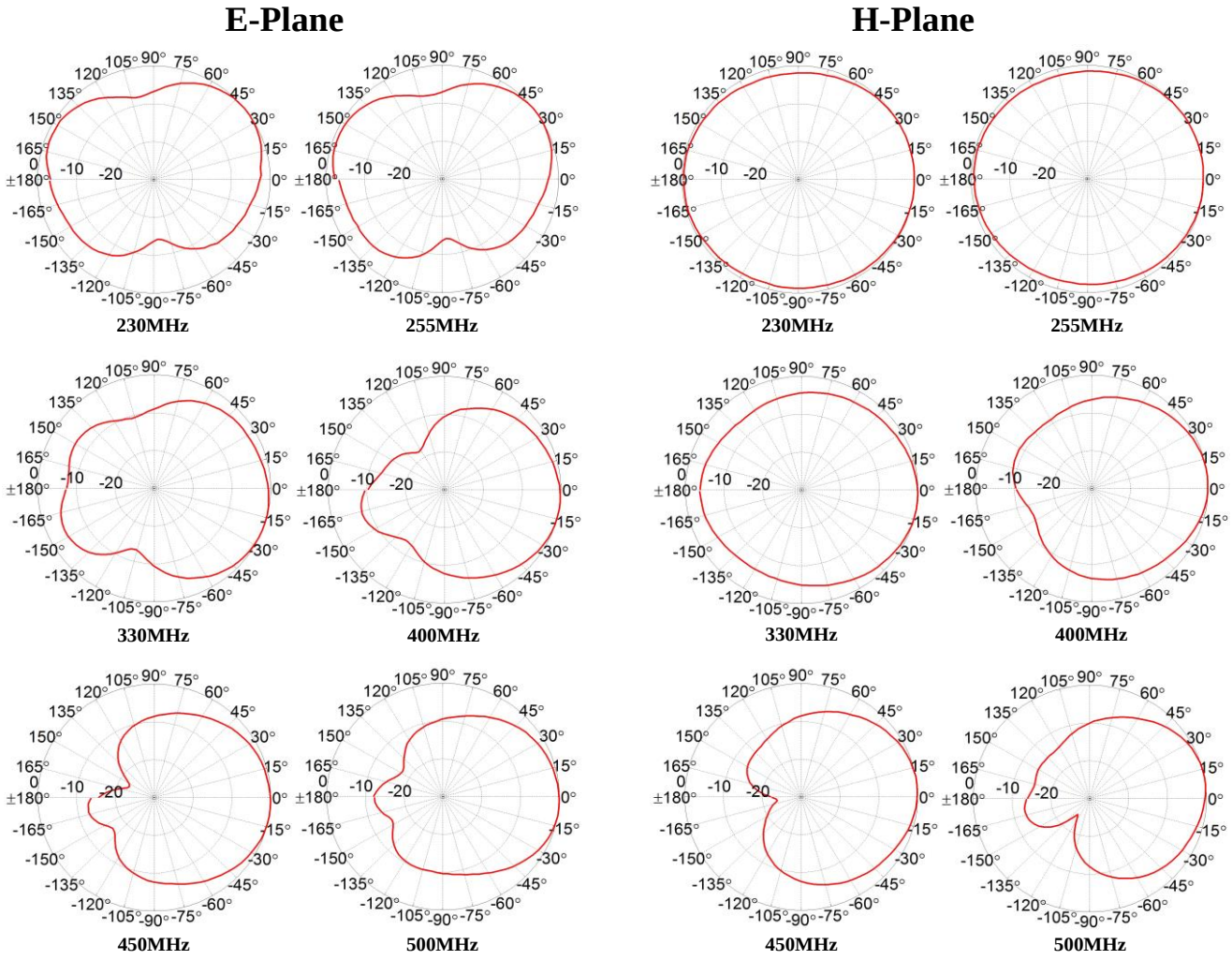

Figure 4.12: a) E-plane and b) H-plane radiation patterns of the final slot antenna design.

(a)

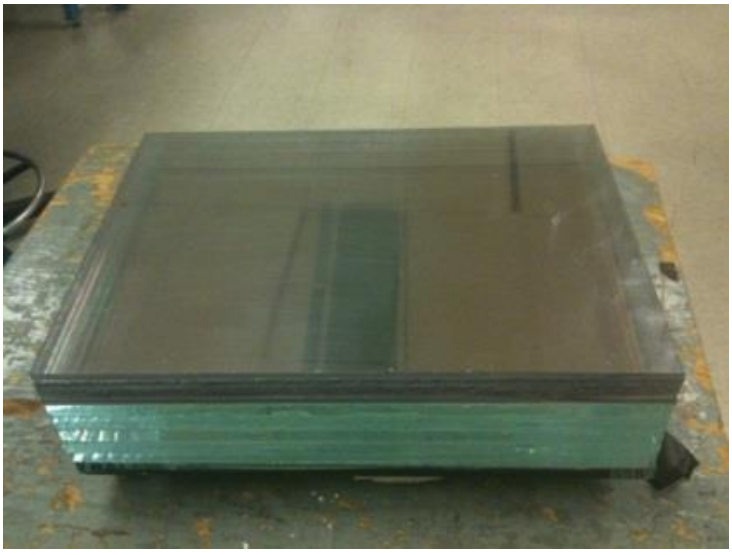

(b)

Figure 4.13: Final design Prototype

4.2 Approach II

4.2.1 Stepped Index Superstrate Design

In this section, very similar steps in designing the antenna to that in Approach I is followed. However, a superstrate with alternated dielectric constants, is used. The electromagnetic waves behavior can be controlled by adding different materials with different permittivities which allows better matching of the waves in the superstrate to the surrounding medium. Adding superstrate with equivalent dielectric constant of periodic media create a dielectric resonance mode near to the other resonance of the slot antenna itself. The superstrate has the effect of reducing the slot dimension for given resonance and therefore, the slot radiates effectively toward the superstrate and reduces the backward radiation. The stepped index allows a better matching to free-space. The width and length of the slot antenna and the thicknesses of each periodic layer of the superstrate are adjusted to achieve the required operating bandwidth.

Figure 4.14 shows the side view of the slot antenna substrate with the glass and the polycarbonate superstrates.

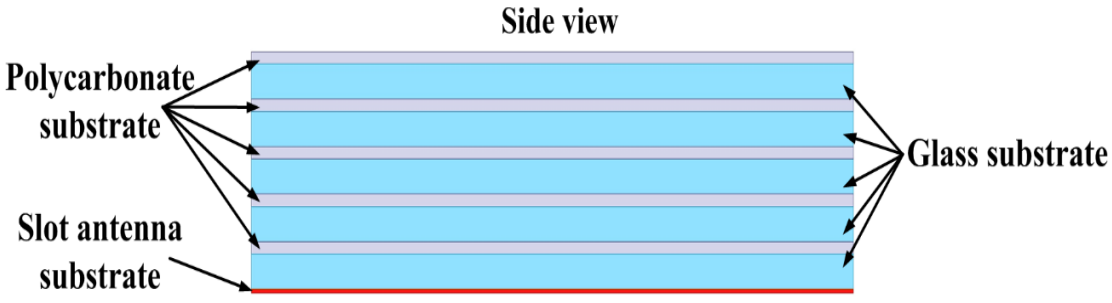

Figure 4.14: The side view of the slot antenna substrate and the stepped index superstrate.

Similar to the previous design in Approach I, two parasitic elements are added to further enhance the bandwidth. Figure 4.15 (a) shows the slot antenna with two parasitic elements above the slot antenna to increase the bandwidth at higher frequency band of operation. Placing the two

parasitic elements close enough to the slot antenna creates strong coupling between the slot antenna and the parasitic elements. The location and dimensions of the two parasitic elements are determined by trial and error method, using the Ansoft HFSS full wave simulator.

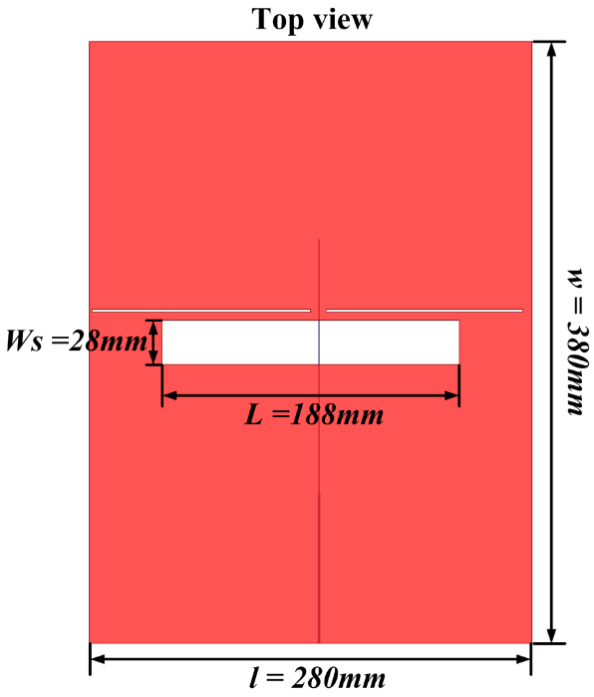

(a)

(b)

Figure 4.15: a) The top view of the slot antenna showing the two parasitic elements. b) The side view of the slot antenna substrate and the graded index superstrate with dimensions.

4.2.2 Measurements and Results

The antenna was fabricated on a Rogers RT/Duroid 5880 substrate with dielectric constant of 2.2 and 0.5mm thickness using the standard PCB technology. The dielectric constant of the glass and the polycarbonate were measured to be 7.2 and 4 respectively. The thickness of each glass layer is 12.7mm and the thickness of each polycarbonate layer is 4.5mm. Different simulations with different numbers of glass polycarbonate layers were performed. Figure 4.16 show the VSWR of the slot antenna with: 86mm, 110mm, 130mm and 150mm superstrate thickness for comparison purposes. 5 layers of Glass and 5 layers polycarbonate are used to assemble the superstrates with stepped dielectric. Therefore, stepped superstrate thickness used is 86mm. Two parasitic elements were added to improve the bandwidth. The dimensions of the parasitic elements were adjusted to achieve the required response. The superstrate is placed on top of the slot antenna as shown in Figure 4.15 (b). Figure 4.17 shows a comparison of the VSWR between the slot antenna with the stepped dielectric superstrate and with the graded index superstrate. The VSWR is then measured using a calibrated HP8720D vector network analyzer. This antenna has a bandwidth of 33.3%. The measured VSWR is compared with the simulate results as shown in Figure 4.18 where a good agreement between the simulation and measured results is observed. The deviation can be attributed to the fabrication process. . Figure 4.19 shows the radiation pattern of the E-plane and H plane. It can be noticed that the radiation is taking place in the front side of the antenna. The back ratio is mainly due to finite size of the ground plane which is higher at lower frequencies.

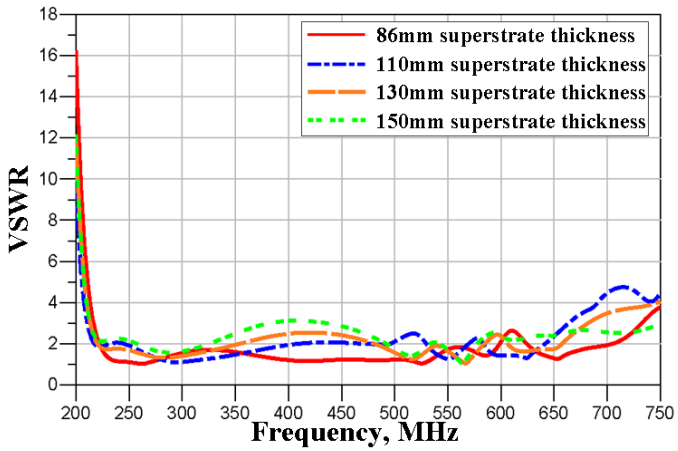

Figure 4.16: comparison of VSWR of the slot antenna with different stepped dielectric superstrate thicknesses.

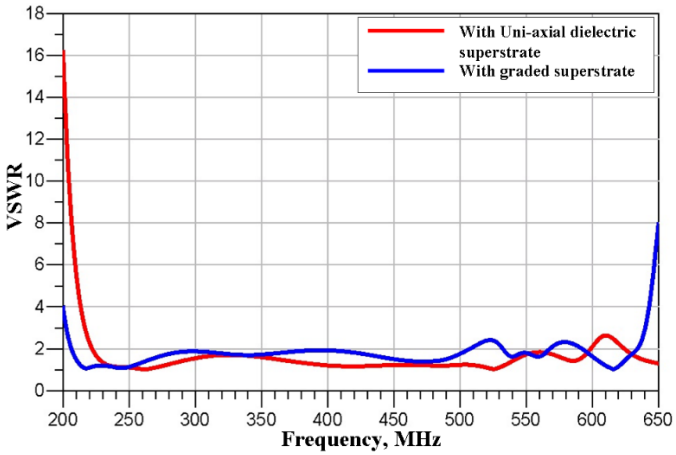

Figure 4.17: VSWR Comparison between the slot antenna with stepped dielectric superstrate and with graded index superstrate.

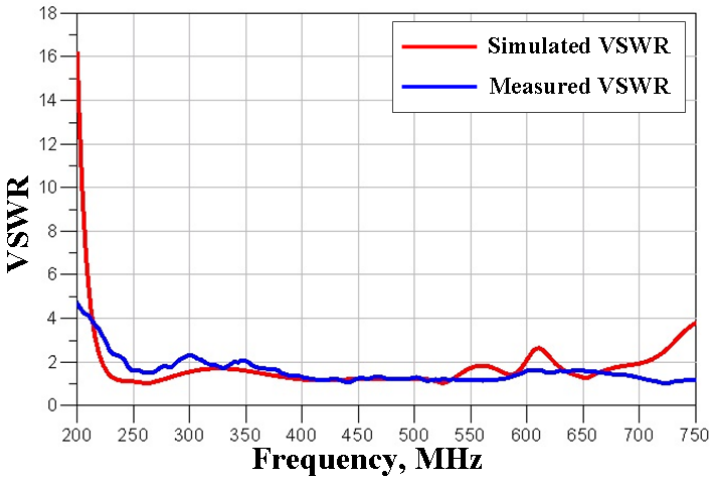

Figure 4.18: measured and simulated VSWR of the slot antenna with stepped dielectric superstrate and two parasitic elements.

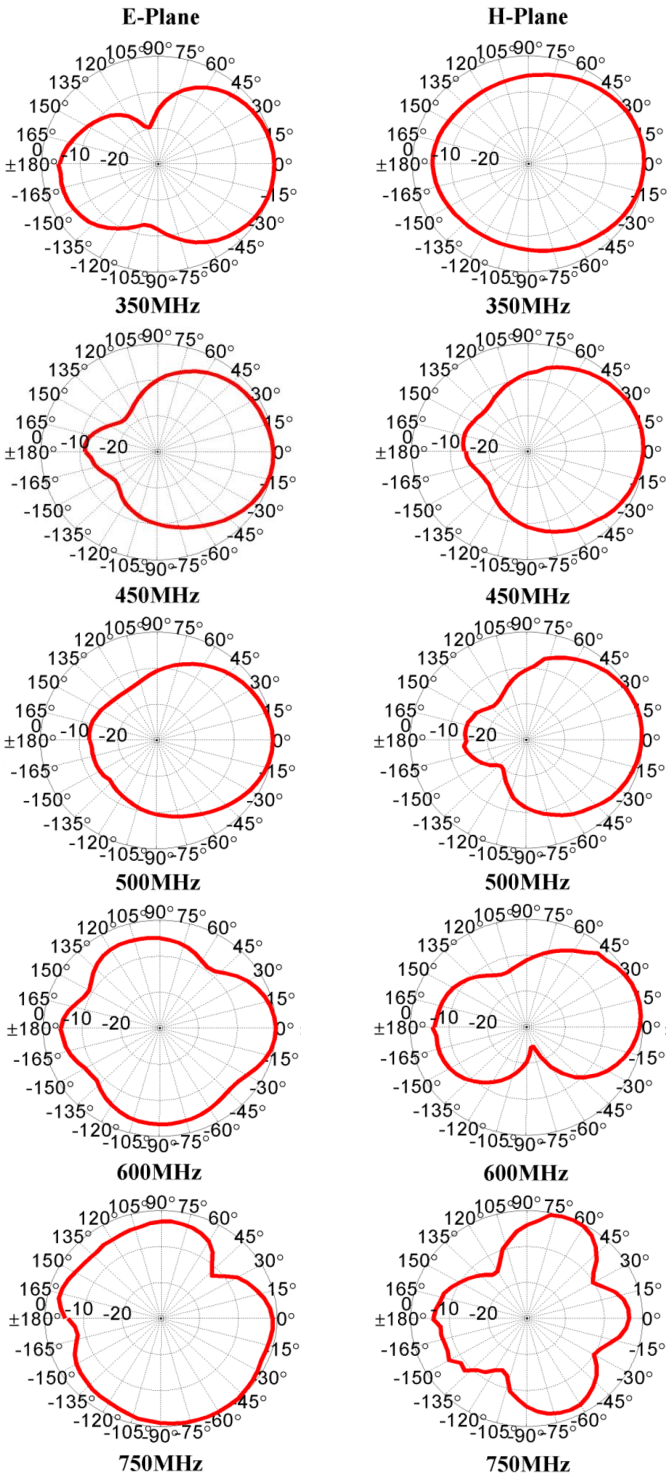

Figure 4.19: E-plane and H-plane radiation patterns of the final slot antenna design.

(a)

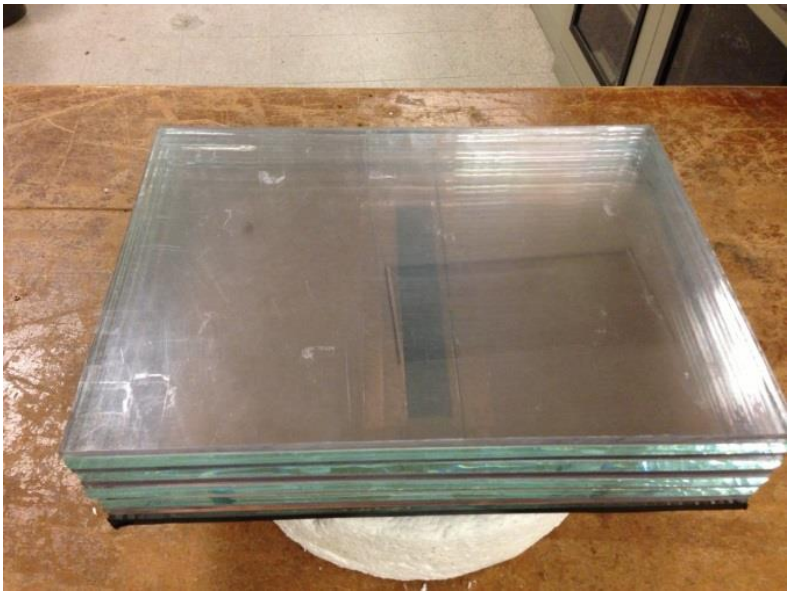

(b)

Figure 4.20: Final design Prototype.

The fabricated slot antenna with a superstrate is then placed directly on sand available in the radiation laboratory at the University of Michigan. Another approach is to add a Styrofoam between the sand and the fabricated antenna as can be seen in Figure 4.21. The reflection coefficients of the antenna placed on the sand itself and sand with Styrofoam are illustrated in Figure 4.22. As can be seen from the figure, there is 10dB difference between the measured antenna and the measured antenna over the sand. However, by knowing the dielectric constant of the sand, the superstrate design can be slightly changed in order to be matched to the given sand.

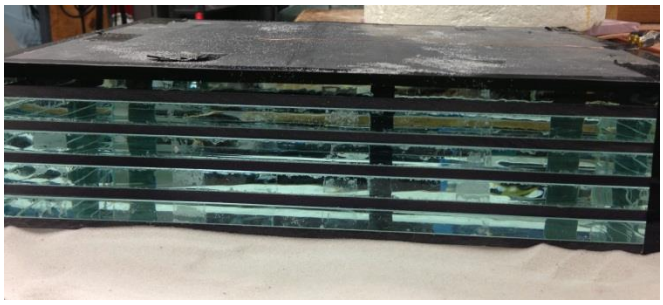

(a)

(b)

Figure 4.21: fabricated antenna on top of; a) sand. b) Sand and Styrofoam.

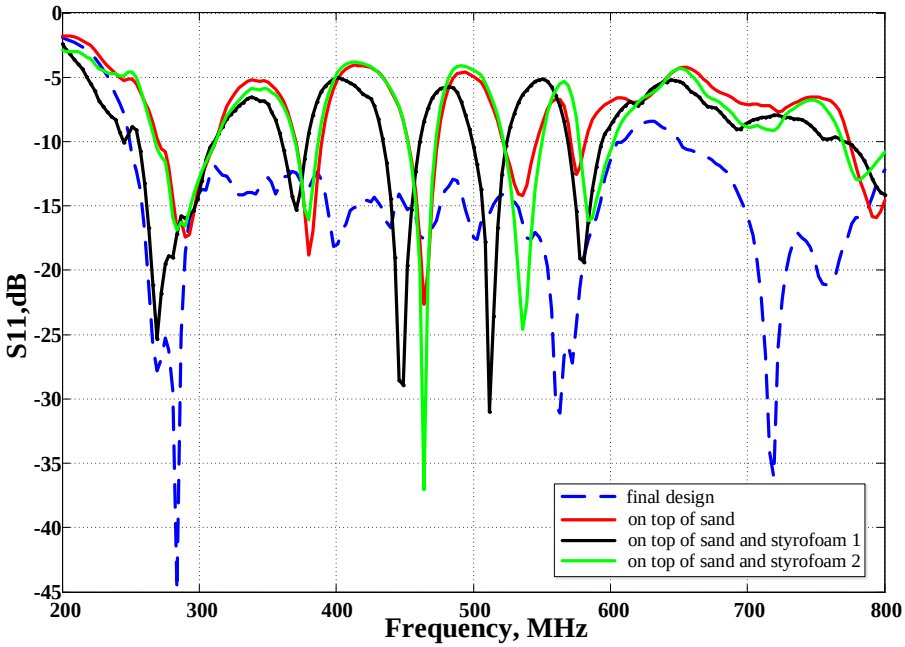

Figure 4.22: Comparison of the measured reflection coefficients of the fabricated antenna on top 1) sand. 2) Sand and Styrofoam.

Another Layer of concrete between the antenna and the sand is added (Figure 4.23). Figure 4.24 shows the reflections coefficient differences between antenna itself, placing the antenna over sand and concrete, and placing the antenna over sand, concrete and Styrofoam.

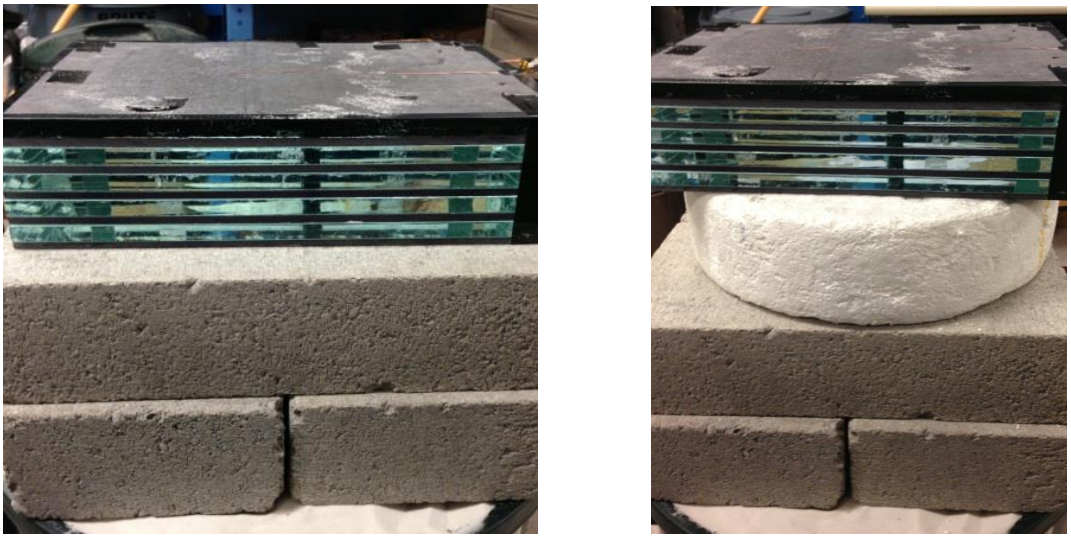

(a) (b)

Figure 4.23: fabricated antenna on top of; a) sand and concrete. b) Sand, concrete, and Styrofoam.

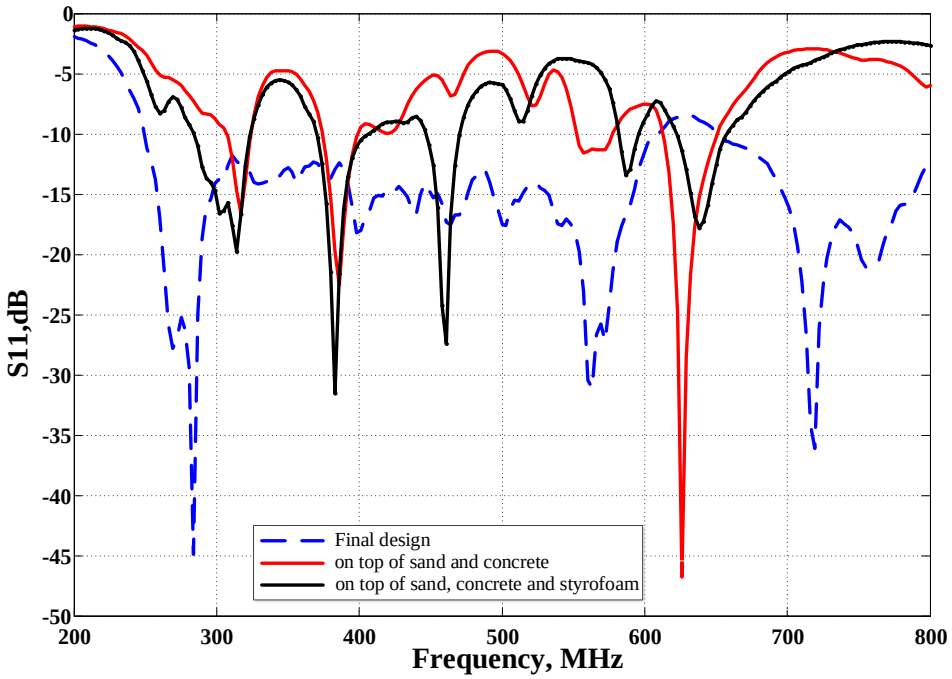

Figure 4.24: Comparison of the measured reflection coefficients of the fabricated antenna on top 1) sand and concrete. 2) Sand, concerete, and styrofoam.

Chapter 5:
Miniaturized Omnidirectional Horizontally Polarized Wire-Loop Antenna

5.1 Background

In addition to the three factors in antenna miniaturization mentioned in sections 1.2.2, generation of a desired polarization or a specific radiation pattern for many application where polarization or radiation diversity are utilized are important. If a horizontal polarization with omnidirectional radiation is desired, a small loop antenna, which the dual of vertical short dipole antenna, can be utilized [56]. However, small loop antennas similar to small dipole antennas are difficult to impedance match to a 50 Ohm line. Use of external matching network may lead to poor radiation efficiency or a bulky antenna structure. Different approaches to reduce antenna size have been reported [57]. One technique to design miniaturized dipole antennas is to meander the wire [58] and [59], however; this approach leads to poor radiation efficiency as the opposite flow of electric current in the meander wire cancel the radiated field from adjacent segments. It is shown in [60]-[62] how the meandering approach can be applied to slot antennas. However, using meandering technique will make the antenna very hard to match to a 50Ω line. Very small slot antennas with very high radiation efficiency that do not require external matching network are reported in [[30], [50] and [63]]. Theoretically slot antennas (with infinite ground plane) should produce omni-directional radiation pattern in E-plane. However, small size slot antennas with finite ground planes produce a null radiation in along the ground plane direction. It is the intent of

this paper to present a small size, low profile, horizontally polarized antenna with omnidirectional radiation pattern that does not require external matching network. Recently, the concept of composite slot loop antenna was introduced to develop a low-profile antenna that can produce a vertical polarization [64]. This antenna design is inspired from a small magnetic loop using a slot configuration on metallic a small ground. For miniaturization purposes, the meandering approach employed in [30] and [63] was utilized to reduce the size of six driven elements around the circumference of a small circle. . The size of this omnidirectional miniaturized antenna can be as small as λ/10 and its height can be as small as λ/60. Since the input impedance of short slot antennas is rather high the elements could be fed in parallel, but series capacitors at the feed point had to be used to achieve the impedance match.

5.2 Antenna Design

It is well-known that a small circular loop can produce horizontally polarized omni-directional radiation pattern. However, a major drawback of this antenna is its extremely low radiation resistance, proportional to $\left(\frac{a}{\lambda}\right)^4$, which is given by [56]:

$$R_{loop} = 320\pi^6 \left(\frac{a}{\lambda}\right)^4 \qquad (9)$$

where, a is the radius of the loop. This low radiation resistance leads to very poor radiation efficiency. Although the radiation resistance can be improved using multi-turn loop (by factor of N^2), the additional ohmic resistance and the resulting higher inductance keeps the radiation efficiency low and impedance matching more difficult. To increase the radiation resistance, the radiated power, which is proportional to the loop current squared, the current in the loop must be increased. This can be accomplished by packing resonant dipole antennas within a circle. To ensure omni-directional radiation, the current around the perimeter of the enclosing circle must be almost

a constant and not canceled by any opposing current. Applying the meandering approach and fold the edge of a half-wavelength dipole antenna into a spiral-like shape reduces the dipole length significantly. Placing these meandered dipole antennas around the circumference of a small circle creates the desired wire-loop antenna as shown in Figure 5.1. It is noted that the circumferential currents, constituted from three diploes, are all in the same direction and almost uniformly distributed around the circle. This is due to the fact that the electric current on a dipole at resonance is strong and almost constant near the feed point. Also feeding the dipoles identically with proper polarity, not only the circumferential currents are uniform around the circle, but also the radiations from the spiral arms of the adjacent dipoles cancel each other. This will cause radiation to only come from the strong circumferential currents as it the case for small wire loop antennas.

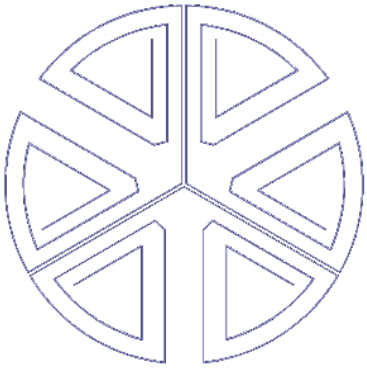

Figure 5.1: Composite wire-loop antenna.

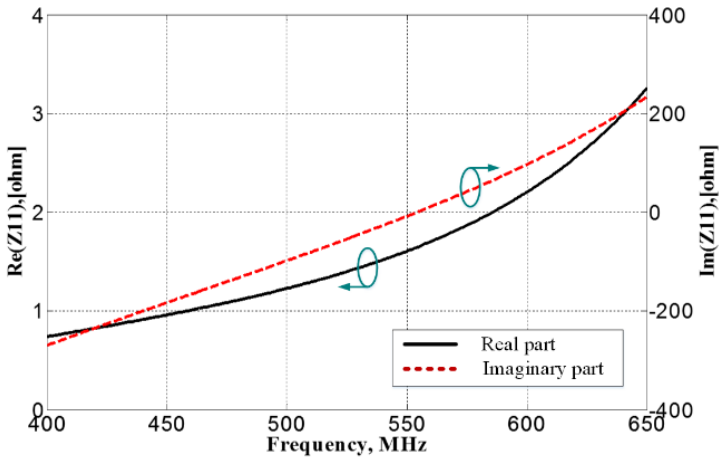

(a)

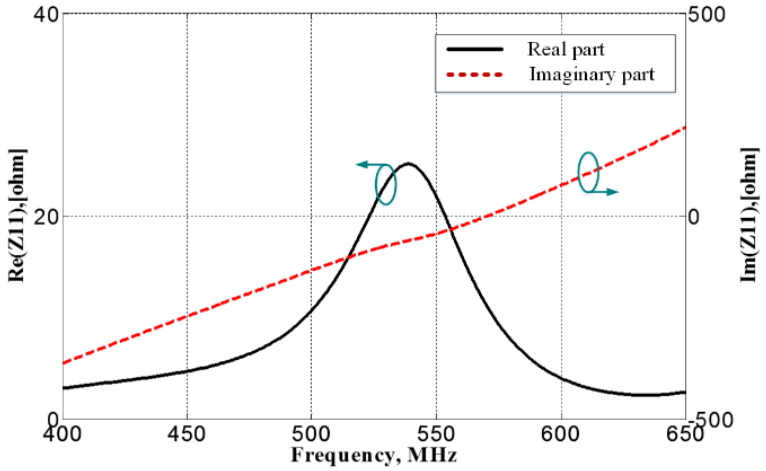

(b)

Figure 5.2: Real and imaginary parts of the input impedance of: a) one short dipole with end spirals and, b) three short dipoles.

The challenges are in the feed network and impedance matching. Short dipole antennas with end spirals have low radiation resistance and rapidly varying reactance at the resonance as shown in Figure 5.2 (a). The terminal is placed right at the middle of the dipole and its physical parameters are as follows: l = 308mm, t = 0.3mm, and h=0.5mm where l is the dipole length and t is the trace width, and h is the substrate thickness with dielectric constant of 2.2. Due to the proximity of the end-spirals, the input impedance and the resonant frequency of a short dipole in the presence of the other dipoles in the composite loop are quite different than the isolated antenna. The input impedance of the dipole of Figure 5.1 in the presence of two other similar antennas terminated with matched load 50Ω is shown in Figure 5.2 (b). One advantage of adjacent elements is that they significantly improve the input resistance and decrease the rate of change of reactance with frequency which leads to higher bandwidth. The most convenient way to feed the antennas is the parallel feeding. Unfortunately, feeding the antenna in parallel fashion will further reduce its input impedance, and matching this antenna to a 50Ω-line becomes very difficult. A better approach is to feed the three antennas in series. This way the radiation

resistances are added and gets closer to the transmission line characteristic impedance. In addition the line thickness and the length of the two wire transmission lines between the dipole terminals and the feed point in the center of the loop can be used for impedance matching as well. To facilitate series feeding approach, the antenna can be fabricated on three layers as shown in Figure 5.3. Metallic via holes can be used to connect the transmission lines to the dipole traces on different layers.

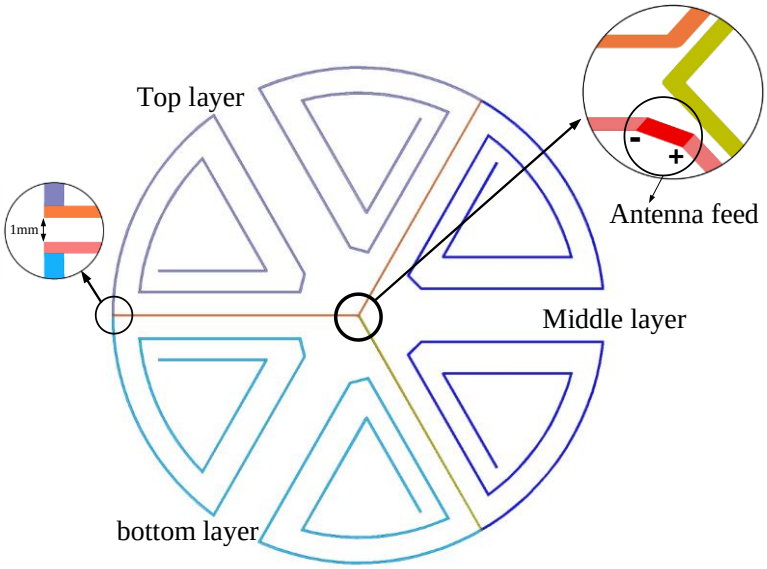

Figure 5.3: Three layers composite-wire loop antenna.

Through extensive numerical optimization it is found that the structure of Figure 5.3 cannot be matched to a 50Ω line exactly. The main problem is the low radiation resistance of the dipoles. One approach is to increase the number of dipoles within the circle. For a given loop radius, each dipole has to be further miniaturized, but this will lead to a very small bandwidth if the antenna could be matched. A better approach for increasing the input impedance is to increase the input impedance of each element using the folded antenna topology. For ordinary dipole antennas the input impedance can be increased with the square of the number of folds. So if there are N parallel

wires forming the multi-folded dipole, the input impedance is increased by N^2 [65]. The geometry of Figure 5.3 is designed and modified for 2-, 3-, and 4-folded short dipoles for the composite loop antenna topology. Figure 5.4 shows the antenna geometry for the 4-folded short dipole configuration. Also Figure 5.5 shows the input reflection coefficients at the feed point of the antenna for 2-, 3-, and 4-folded configurations. As observed the input impedance of the folded structure can be better matched with higher bandwidth when the number of folds increased. The shift in the resonant frequency is the result of change in the mutual coupling between the adjacent elements. It should be emphasized that the diameter of 4-folded configuration is less than λ/9 at the resonant frequency. The simulated gain of the antenna is 0.2dB and its radiation efficiency is 90% which is by may order of magnitude higher than the conventional small loop antennas.

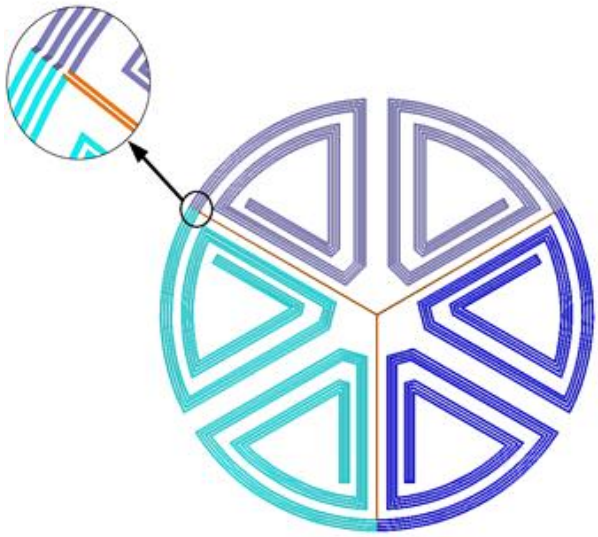

Figure 5.4: Folded Composite wire-loop antenna.

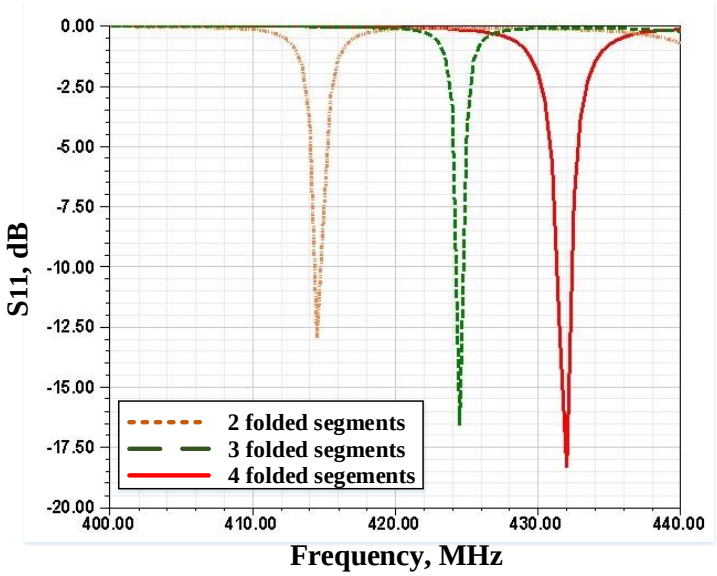

Figure 5.5: The reflection coefficient of the composite wire-loop antenna with different folding numbers.

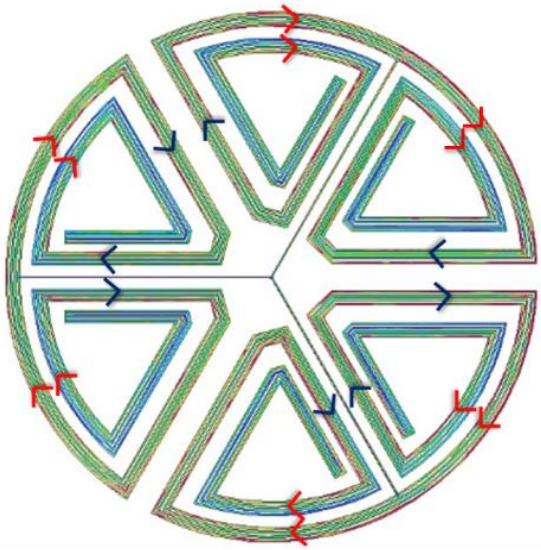

Figure 5.6: The current distribution over the composite loop antenna.

5.3 Antenna Feed

Connecting a dipole antenna directly to a coaxial cable induces electric current over the outer layer of the coaxial cable which in turn can cause radiation and unbalanced current distribution on the dipole arms. A transformer with a center-tap terminal of its secondary coil connected to the outer connector of the input coaxial line which is connected to the primary coil of the transformer,

produces a balance terminal (the transformer secondary) for the dipole. The advantages of transformer-type baluns is their compact size and light weight which make them ideal for application at HF-UHF bands [65] and [66]. This is important as the size of the antenna is very small compared to the wavelength. For lower frequency applications, the size of transmission line baluns are quite large (>λ/4) and cannot be used. Therefore, an isolated balanced to unbalanced transformer is suggested and used. In this design, a 3.8mmx3.8mm mini wideband transformer from coilcraft, WBC1-1TLB, with 1:1 impedance ratio and 0.58dB insertion loss is used. Due to space limitation, a MMCX jack connector is used instead of a regular SMA connector. This connector is then connected to MMCX to SMA adapter for cable connections during measurements.

5.4 Measurements and Results

The designed antenna is fabricated on a 0.5mm thick RT/Duroid5880. This substrate has a dielectric constant of 2.2 and loss tangent of 0.0009. Two parts of the proposed antenna were fabricated on opposite sides of one substrate. The third part of the antenna was fabricated on a second substrate which is then limited to the first substrate. The fabricated antenna overall diameter is 77.6mm with a height of 1mm. Figure 5.7 shows the top view of the antenna final design with dimensions. Figure 5.8 shows the final design prototype. The figure shows each layer individually since each layer is on a different substrate surface.

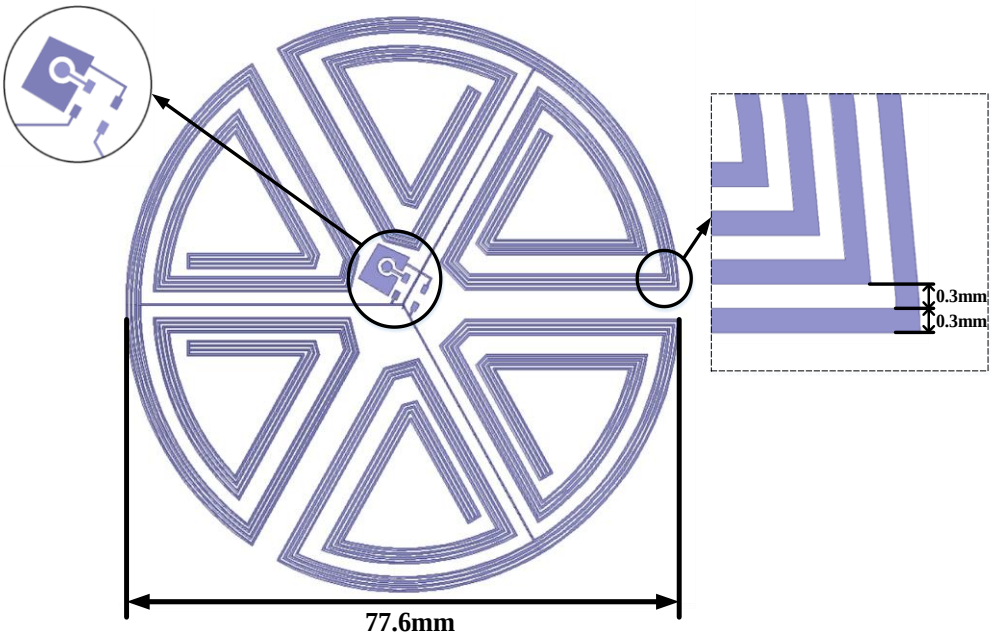

Figure 5.7: The composite wire-loop antenna with the transformer and MMCX jack connector pads.

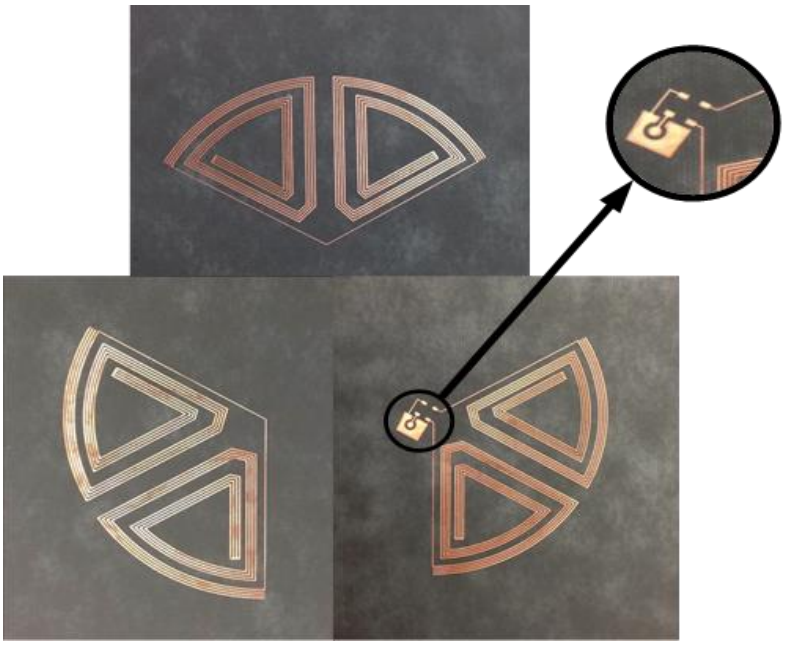

Figure 5.8: The prototype of the composite wire-loop antenna.

The reflection coefficient of the fabricated antenna is measured using a calibrated HP8720D vector network analyzer. Figure 5.9 shows the measured and simulated reflection coefficients. It

is shown that the measured result is in a good agreement with the simulation. However, the deviation can be attributed to the fabrication process. The radiation pattern is measured using the University of Michigan Radiation Laboratory anechoic chamber. Figure 5.10 shows the measured radiation pattern of the composite wire-loop antenna in the E and H planes and as expected the far-filed radiation pattern very closely resembles that of a small dipole. The radiation pattern in E-plane is uniform to within ±0.25dB. Also the antenna gain is measured to be 0dBi. Comparing the measured gain with the directivity of an ideal small loop antenna (1.75dB), the antenna radiation efficiency (including the balun loss) is found to be 67% which is far better than conventional small loop antennas.

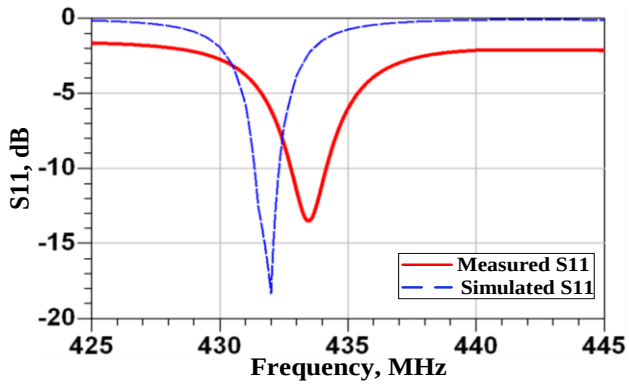

Figure 5.9: The measured and simulated reflection coefficients of the composite wire-loop antenna.

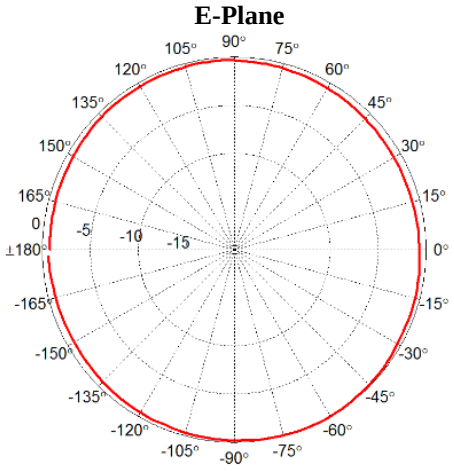

(a)

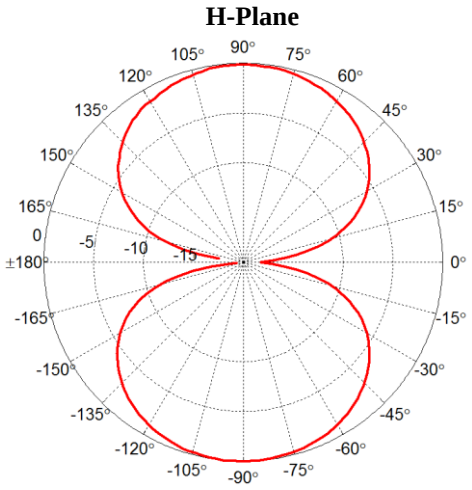

(b)

Figure 5.10: The measured radiation pattern of the composite wire-loop antenna. a) E-Plane. b) H-Plane.

Chapter 6:
A compact, Wideband Array of Coupled Quarter-Wavelength Slot Antenna for the 700MHz band

6.1 Quarter wavelength slot antenna

A relatively new approach to reduce the slot antenna dimensions is to shorten the antenna length to λ/4 instead of λ/2 and have one edge open. This new approach is similar to the inverted-F antenna. Quarter-wavelength slot antenna is also called monopole slot antenna [67] and [68]. A λ/4 slot antenna with one end open circuited and the other short-circuited is fed by a microstrip feed line and used as the driving element is presented. This antenna is based on the basic half-wavelength slot antennas. The mechanism of designing the quarter-wavelength slot antenna is to use one half of the half-wavelength slot antenna and to have one of the slot edges as an open circuit. Using this concept, the size of the antenna is reduced by half and the resonant frequency is remained unchanged. A number of λ/4 slot antennas are appropriately position around the driving element to achieve the required bandwidth. An advantage of this design is that active circuit components can be place on the top side of the substrate that supports the microstrip line as long as the slots are not covered or crossed by RF lines.

6.2 Antenna design

A quarter-wavelength slot antenna is based on the basic half-wavelength slot antenna. A resonance can be achieved if half of the half-wavelength slot antenna is used. This supports the

maximum voltage at the open end and a voltage node at the short circuit end. Unlike quarter-wave monopole antennas that require a ground plane, quarter-wave slot can easily be realized on a finite ground plane as shown in Figure 6.1 (a). Similar to half-wavelength slot antennas can be easily excited and matched to a wide range line impedances, by a microstrip line crossing the slot near one end. The closer the line crossing point to the short-circuited end, the lower the input impedance will get. The reactance of the slot antenna can also easily be compensated by choosing the length of the open-ended mircostrip line extending beyond the slot crossing point. Figure 6.1 illustrates a λ/4 slot antenna design that has a center frequency at 700MHz as can be seen from the reflection coefficient shown in Figure 6.1 (b). However, the location and dimension of the microstrip feed line was adjusted using the Ansoft HFSS simulator to achieve the desired resonant frequency. This response is similar to the response of the conventional λ/2 slot operating in the same frequency.

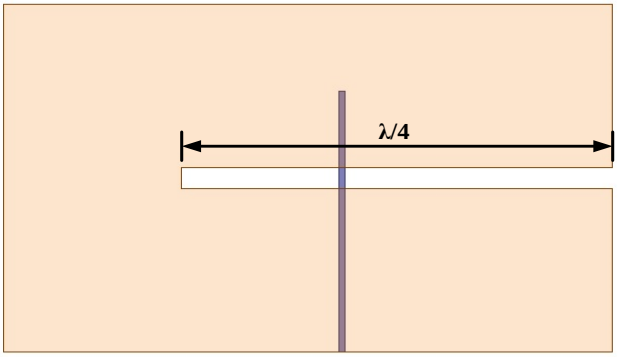

(a)

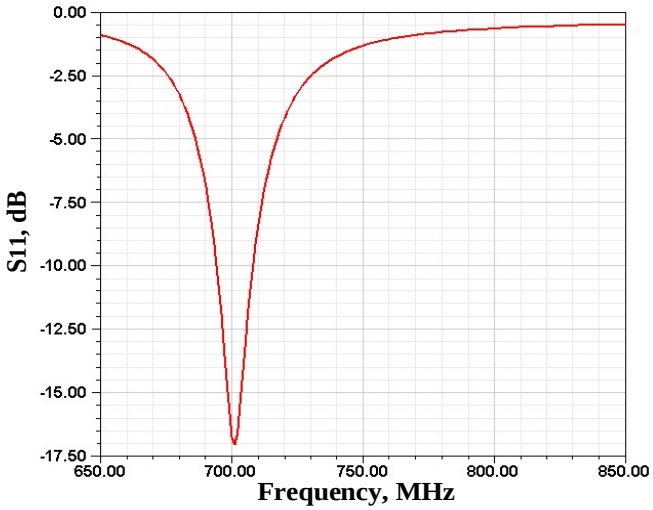

(b)

Figure 6.1: a) Quarter-wavelength slot antenna design. b) The reflection coefficient of the quarter-wavelength slot antenna.

6.3 Double-element quarter-wavelength slot antenna

Enhancing the bandwidth by using a double-element conventional slot antenna was studied and reported in [43]. In this section, two quarter-wavelength slot antennas, operating at slightly different frequencies, using a single microstrip feed line to feed both slot antennas is presented. This topology is similar to the multi-band microstrip feed line slot antenna discussed in section 3.2. As mentioned in section 3.2.1, there are number of different multi-element feeding topologies. The parallel feed topology is a great alternative for multi-element antenna since it provides better flexibility in designing the feeding network as it makes the antenna impedance matching easier to be achieved. Figure 6.3 shows the geometry of a two-element quarter-wavelength slot antenna fed in parallel with a microrstrip line. The impedance match and the resonant frequencies are achieved by the feeding line cross points, the open-ended microstrip stub lengths, and the length of the slot antenna elements.

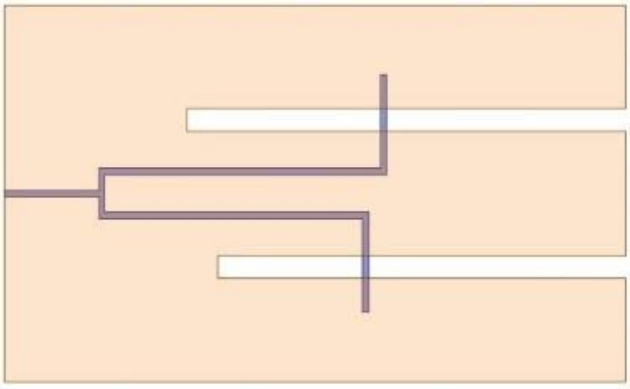

Figure 6.2: Quarter-wavelength double-element slot antenna design.

A third resonant is near 800 MHz, shown Figure 6.3, is also observed. This was initially assumed to have been generated from a fictitious short circuit reported in [43]. Under certain conditions, microstrip fed slot antennas can produce two resonances. This second resonance is attributed to a fictitious short circuit within the slot generated from the cancellation of field produced by the feeding line and the field of the slot line. Our attempts to generate such resonance in quarter-wavelenght slot antennas were not successful. Running more simulations, it is found out that the additional resonance remains even after removing the second λ/4 slot antenna while keeping the second microstrip feeding line as can be seen in Figure 6.4. It is suggested that the additional feed line leg is effecting the impedance matching which create the third resonant at a higher frequency. Figure 6.5 shows the reflection coefficient of a single λ/4 slot antenna with different length values of the additional microstrip feed line. As can be seen from this figure, changing the length of the feed line changes the antenna input impedance.

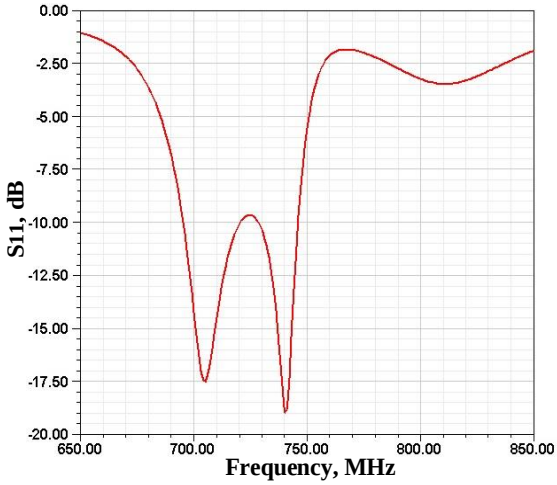

Figure 6.3: The reflection coefficient of the quarter-wavelength double-element slot antenna

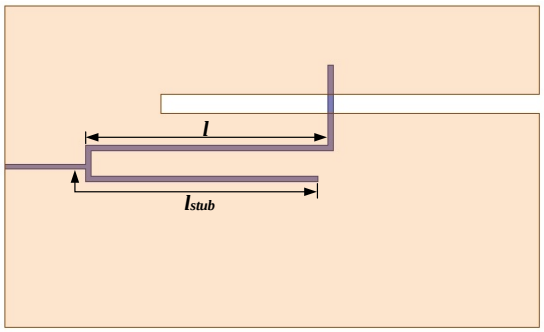

(a)

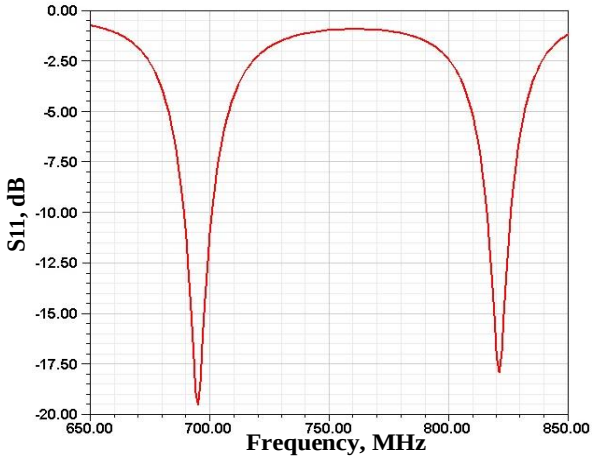

(b)

Figure 6.4: a) Single quarter-wavelength slot antenna with additional feed line. b) The reflection coefficient of the quarter-wavelength slot antenna with the additional feed line.

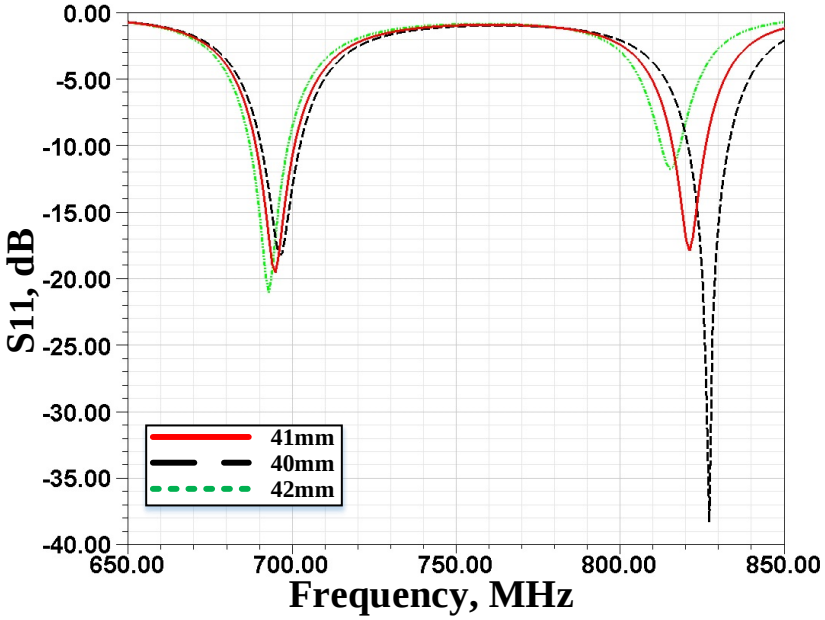

Figure 6.5: The reflection coefficient of the quarter-wavelength slot antenna with different lengths of the additional feed line.

To get a better impedance-matched condition, the length of the second microstrip line is adjusted. This is interesting as it is shown that an open-ended microstrip line can make the impedance matching possible at two frequencies. One of the popular matching approaches is to use an open-circuited stub of appropriate length at an appropriate distance from a load [69]. There are two adjustable parameters in the shunt stub topology, the distance from the load to the shunt stub (l) and the shunt length (l_{stub}) as illustrated in Figure 6.4 (a). Figure 6.7 shows the input impedance of the microstrip line as a function of frequency without adding the shunt stub as demonstrated in Figure 6.6. For wideband operation a frequency near the end of the band is considered and stub matching approach is used to match the antenna at that frequency.

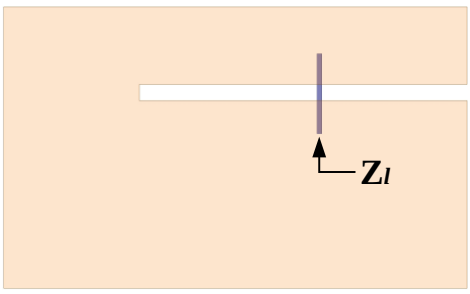

Figure 6.6: Single λ/4 slot antenna design showing the input impedance, Z_l, location.

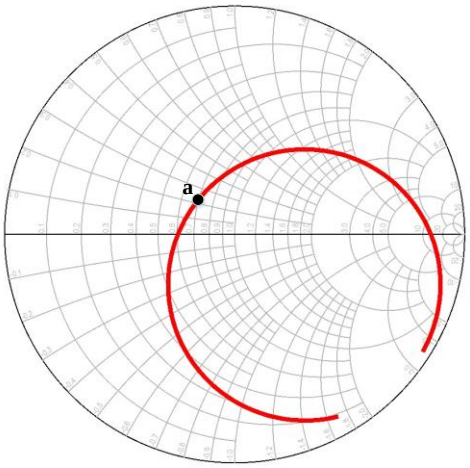

(a) is at 700MHz

Figure 6.7: Smith chart of single λ/4 slot antenna design.

Both distances, l and l_{stub}, were optimized to improve the matching at the beginning and the end of the desired band of operation. Figure 6.8 shows how the antenna impedance as a function of frequency with two impedance matched frequencies of 695MHz and 821MHz.

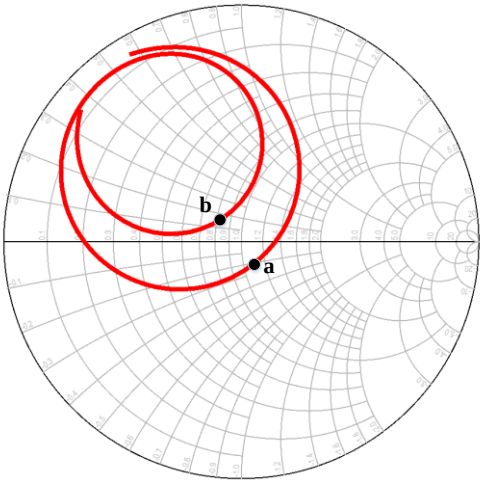

(a) is at 695MHz
(b) is at 821MHz

Figure 6.8: Smith chart of single λ/4 slot antenna design with the shunt stub.

6.4 Bandwidth enhancement with additional parasitic elements

Another technique to increase the antenna bandwidth is to add parasitic elements. A number of λ/4 slot antennas are appropriately positioned around the driving element to achieve the required bandwidth. The entire structure is designed over a finite ground plane whose dimensions also affect the resonant frequencies and eventually the overall bandwidth of the antenna. As shown in Figure 6.4, an open stub is needed to get a resonance at the upper portion of the band. To eliminate the possibility of interaction of this stub with other parasitic elements, the microstrip stub is meandered in a corner as shown in Figure 6.9. Figure 6.9 (a) illustrate the λ/4 slot antenna with one parasitic element while Figure 6.9 (b) shows the effect of the single parasitic element on the antenna's reflection coefficient. The parasitic element's length and separation from the driven element are adjusted to achieve the second resonance. As can be seen, the meandered microstrip stub is also creating the third resonant at 830MHz.

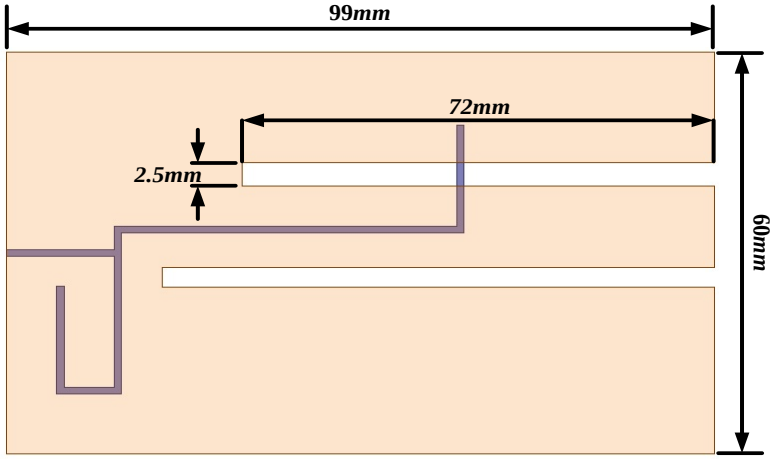

(a)

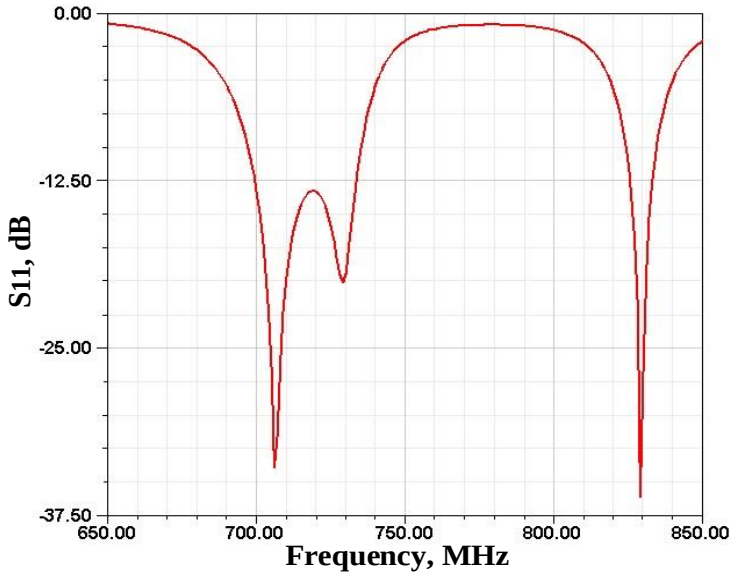

(b)

Figure 6.9: a) λ/4 slot antenna with single parasitic element. b) The reflection coefficient of the λ/4 slot antenna with single parasitic element.

To fill the spectrum with resonance and achieve a wideband, more parasitic elements are needed. The location and the number of elements are determined from the current distribution on the ground plane. After extensive numerical optimization, it is noticed that changing the length of the microstrip stub not only affects the location of the resonant frequency created by this stub, but also affects the location of the other resonances created by the parasitic elements. This is due to the fact that the reactance of the driven slot antenna is affected by the presence of the parasitic elements. Figure 6.10 shows the input reflection coefficient of the slot antenna with different numbers of parasitic elements. The number of resonances observed is equal to number of parasitic elements plus two. One resonance is due to the driven elements and the other is due to the mirostrip stub. It is noted here that the antenna parameters with 1, 2, or 3 parasitics are optimized individually arrive at the results shown in Figure 6.10. It turned out that to achieve the required bandwidth 4 parasitic elements are required.

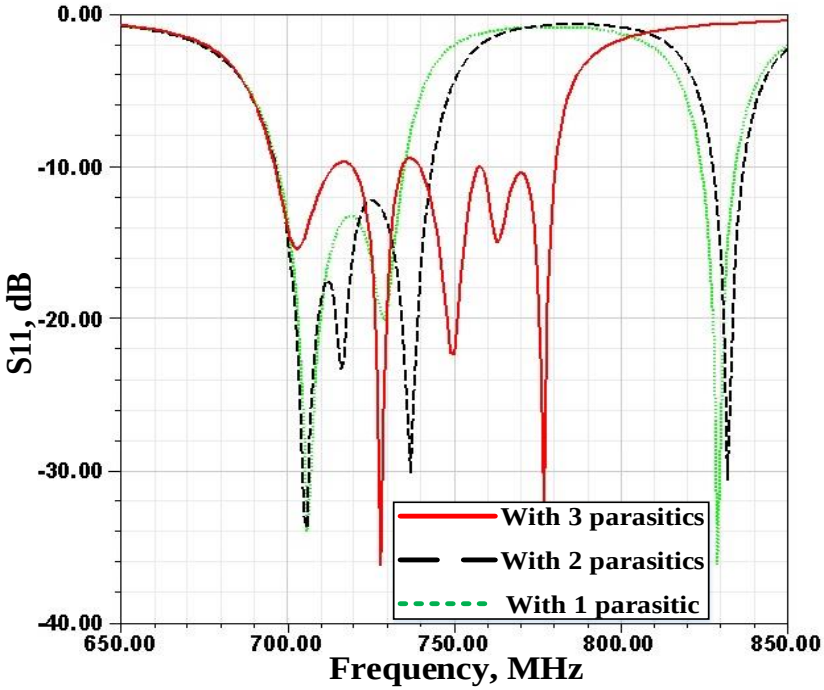

Figure 6.10: The reflection coefficient of the λ/4 slot antenna with different parasitic element numbers.

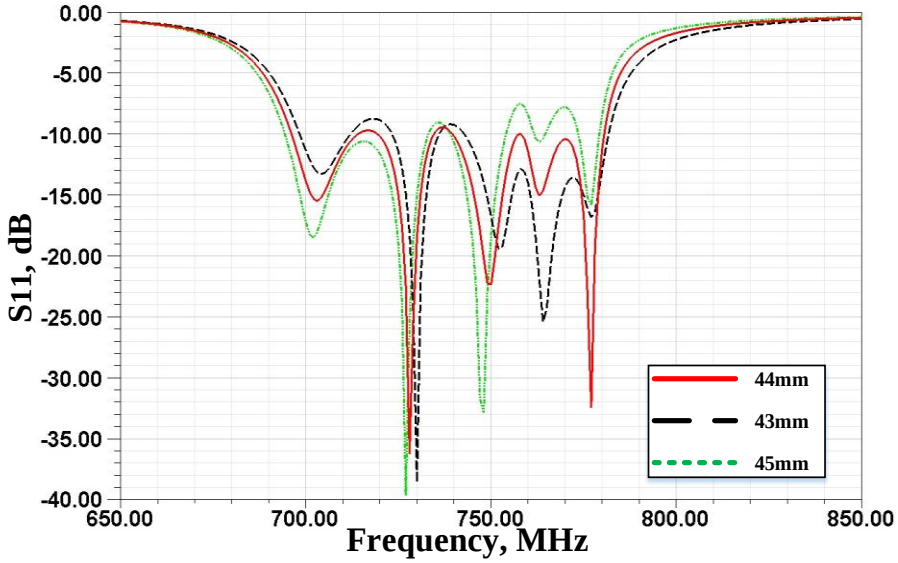

Figure 6.11: The reflection coefficients of the λ/4 slot antenna with 3 parasitic elements and different additional feed line leg lengths.

Figure 6.11 shows how changing the length of the additional microstrip feed line effects antenna input impedance. A fourth parasitic element is added close to the existed three parasitic

elements. Figure 6.12 shows the configuration of the final design. The input impedance of this antenna with 6 resonances is shown Figure 6.13.

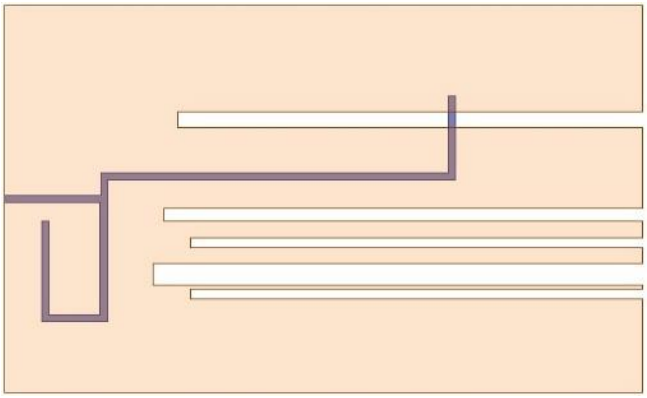

Figure 6.12: The final design of the λ/4 slot antenna with 4 parasitic elements.

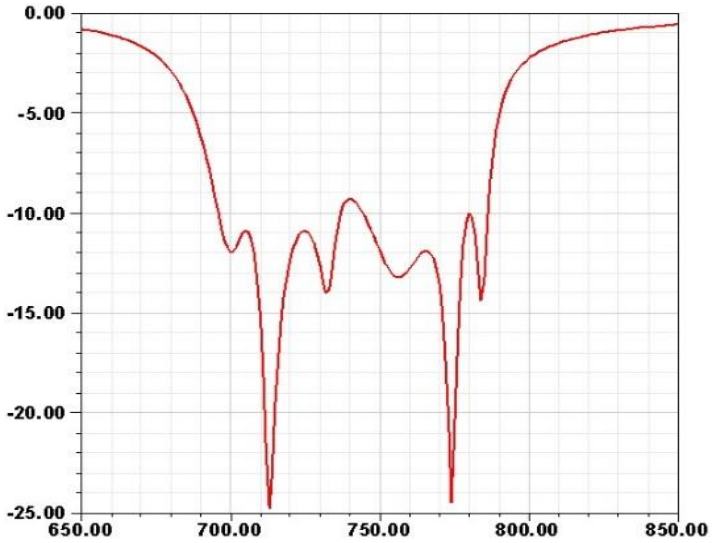

Figure 6.13: The simulated reflection coefficient of the λ/4 slot antenna with 4 parasitic elements.

6.5 Measurements and Results

The designed antenna is fabricated on a 0.8mm thick FR-4 substrate. This substrate has a dielectric constant of 4.4 and loss tangent of 0.02. Both sides of the substrate were used, top side for the slot antenna with all four parasitic elements and the bottom side for the microstrip feed line. The overall dimension of the substrate is 99*mm* x 60*mm* x 0.8*mm*. Figure 6.14 shows the fabricated antenna size, top and bottom views, compared to an Apple iPhone.

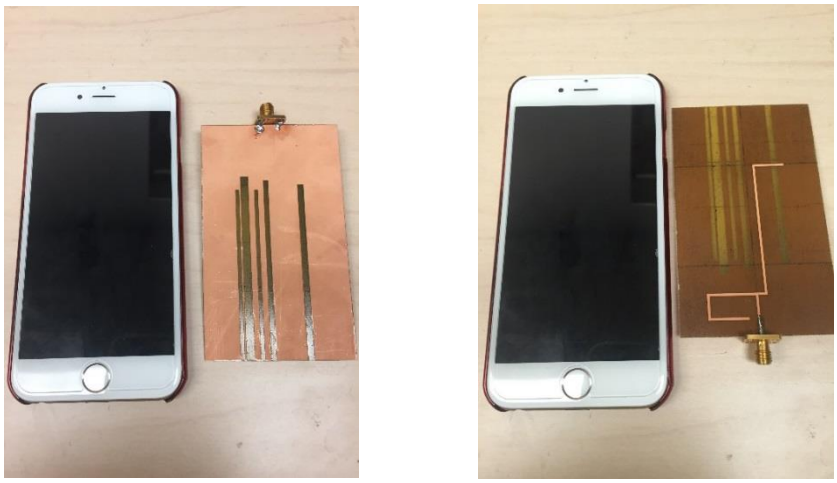

Figure 6.14: Top and bottom views of the fabricated quarter-wavelength slot antenna next to an Apple iPhone device.

The reflection coefficient of the fabricated antenna is then measured using a calibrated HP8720D vector network analyzer. Figure 6.15 shows the measured and simulated reflection coefficients. It is shown that the measured results are in a good agreement with the simulation. However, the small differences between the measured and simulated reflection coefficient can be related to the fabrication process. Figure 6.16 shows the measured gain is in a good agreement with the simulations as well. The radiation pattern is also measured using the University of Michigan Radiation Laboratory anechoic chamber. Figure 6.17 (a) and (b) show the measured radiation pattern of the proposed antenna in the E and H planes respectively.

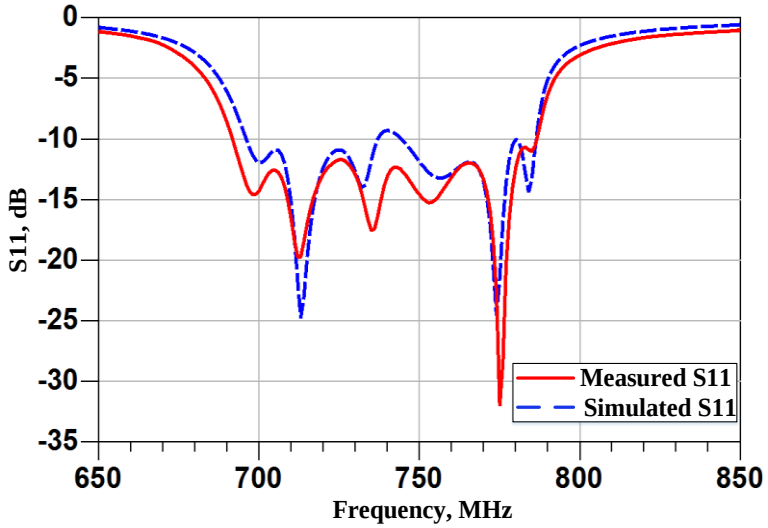

Figure 6.15: Measured and simulated reflection coefficients of the quarter-wavelength slot antenna.

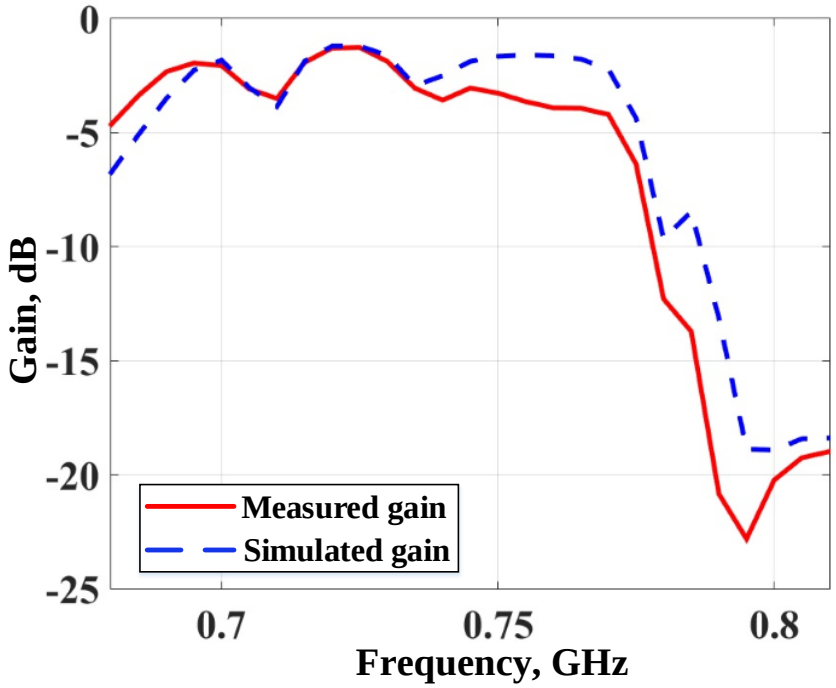

Figure 6.16: Measured and simulated gain of the quarter-wavelength slot antenna.

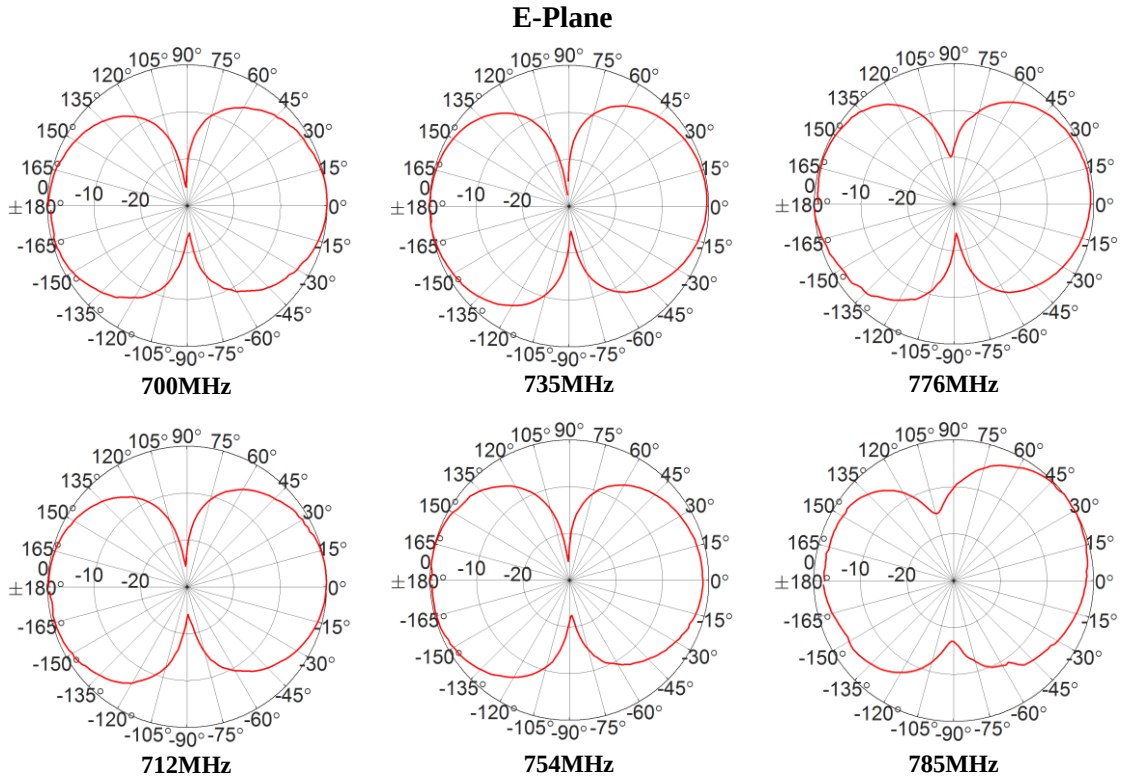

(a)

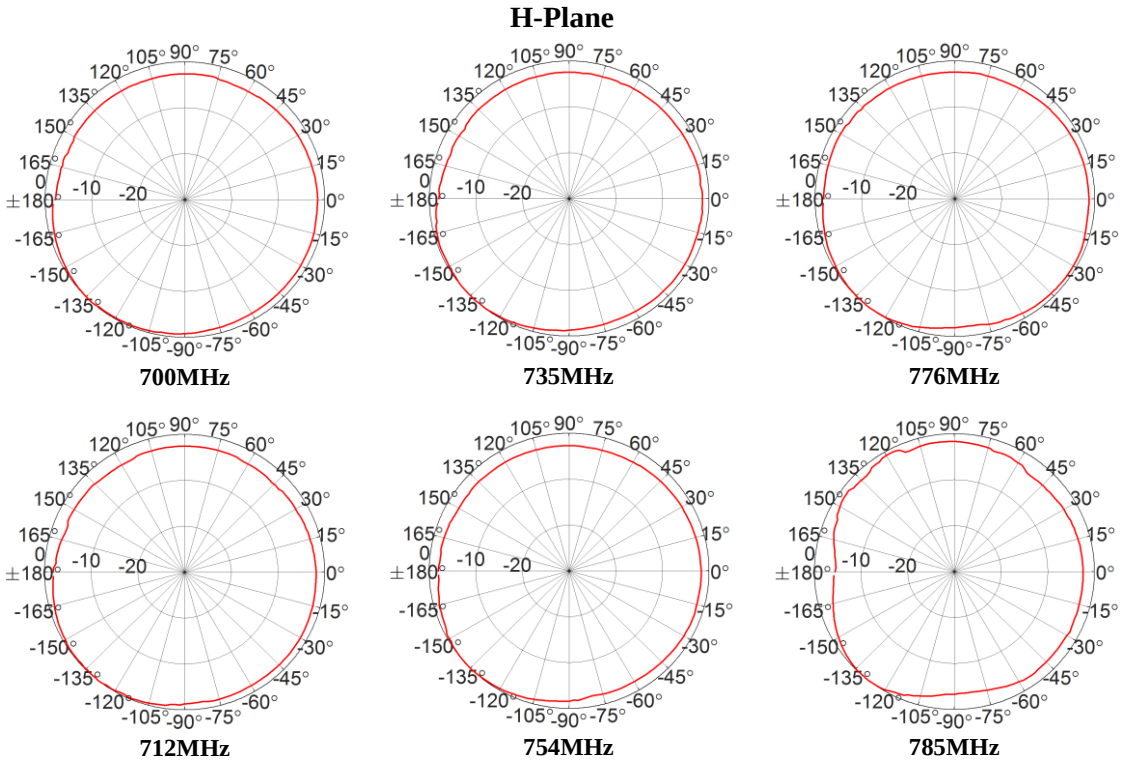

(b)

Figure 6.17: Measured radiation pattern of the quarter-wavelength slot antenna. a) E-Plane. b) H-Plane.

Chapter 7:
Conclusion and Future Work

In this Thesis, we have introduced several antenna designs that are suitable for different applications, mainly for ground penetrating radar or wireless communication applications. Some of these antennas are a continuous work for previous designs such as the coupled sectorial loop antenna (CSLA). All the antennas introduced in this thesis were fabricated and measured in the Radiation Laboratory at the University of Michigan.

7.1 Directional coupled sectorial loop antenna

A modified ultra-wideband coupled sectorial loop antenna is designed. This antenna is based on the concept of omnidirectional coupled sectorial loop antenna. Different methodologies were applied to improve the directivity of the antenna and to enhance the bandwidth. It has a VSWR lower than 2.5 across a 2.7:1 frequency range without the use of absorbing foams or lossy elements. The diameter of this antenna is approximately $\lambda/2$ at the lowest frequency of operation while the height of the antenna is $\lambda/5$. This antenna is then fabricated and measured in the Radiation Laboratory at the University of Michigan. Rogers RO4003C substrate of 1.5mm thickness and dielectric constant of 3.38 were used in fabricating the CSLA, the parasitic and the fin. Rogers 3003 of 0.127mm thickness and dielectric constant of 3.00 were used in fabricating the cylindrical cavity. The measurement results show that the operating frequency is from 0.75 GHz to 2.0 GHz with VSWR lower than 2.5, and S_{11} is better than -7.4 dB.

7.2 Quadruple-element slot antenna

A new approach in enhancing the bandwidth of a slot antenna is presented. This approach includes increasing the number of slot elements. Each element operates in a different band of operation. As a result, a very wide bandwidth antenna is observed. The off-centered microstrip feed line is applied to each slot element. In order to feed the four elements using a single feed, a parallel feed topology is used. The antenna is fabricated using Rogers RO4350 substrate with a dielectric constant of 3.4 and loss tangent of 0.0037. The dimensions of the substrate is as follows: length of 470mm, width of 210mm, and thickness of 0.5mm. The VSWR was then measured using a calibrated HP8720D vector network analyzer. The antenna shows a frequency range of 8.5:1. It is noticeable that the measured result is in a good agreement with the simulation. However, the deviation can be attributed to the fabrication process.

7.3 Slot antenna with graded index superstrate

Two different approaches in designing an ultra-wideband slot antenna with graded index superstrate are presented. The wide bandwidth is obtained by combining three techniques: 1) creation of a fictitious short in a relatively wide slot, 2) inclusion of parasitic slots, 3) utilization of a superstrate with graded index as a dielectric resonator antenna. The use of a stepped index dielectric superstrate facilitates higher bandwidth and better match to free space. Both slot antennas of the two approaches have the same dimension so are the dimensions of the substrates.

The first approach has a stepped index superstrates with tapered dielectric constants, from dense to sparse and four parasitic elements is designed. The antenna shows a frequency range of 2.9:1 with directional radiation pattern. A prototype was also fabricated and measured. Rogers RT/duroid 5880 substrate of 0.5mm thickness and dielectric constant of 2.2 was used as the substrate of the slot. Glass and polycarbonate are used to assemble the stepped index superstrates

with tapered dielectric. The dielectric constant of the glass and the polycarbonate were measured to be 7.2 and 4 respectively. The thickness of the glass is 72mm and the thickness of the polycarbonate is 22mm. Four parasitic elements were added to improve the bandwidth. The dimensions of the parasitic elements were adjusted to achieve the required response.

The second approach has a superstrate with alternated dielectric constants and two parasitic elements. Similar to the first approach, the antenna was fabricated on a Rogers RT/duroid 5880 substrate with dielectric constant of 2.2 with 0.5mm thickness. Five layers of glass with 12.7mm thickness of each layer and five layers of polycarbonate with 4.5mm thickness of each layer are used. The total thickness of the superstrate is 86mm. the dimensions and location of the two parasitic elements were modified to obtain the desired response. The fabricated antenna shows a frequency range of 3:1.

For Future work, by knowing the dielectric constant of the sand, the graded index superstrate can be designed to allow better matching to the sand and reduces the quality factor of the dielectric resonator. The weight of the superstrate is heavy due do that fact that part of the fabricated superstrate is made of glass. To reduce the weight of the superstrate, we can substitute the glass with another material that has the same dielectric constant but lighter than the glass such as rogers substrates.

7.4 Composite wire-loop antenna

A new approach of designing a miniaturized, horizontally polarized, omnidirectional antenna is presented. In this approach, a composite wire-loop antenna composed of three miniaturized resonant folded dipole antennas arrange around the circumference of a small circle is conceived. It is shown that by a serial feed network of proper length and line impedance, the antenna can easily matched without any external matching network. A prototype was fabricated

and its radiation pattern and input impedance were measured. The antenna was fabricated on a 0.5mm thick RT/Duroid5880 with a dielectric constant of 2.2 and loss tangent of 0.0009. The measurements show very good agreement with simulated results. Omni-directional radiation pattern in E-plane with ±0.25dB variations was demonstrated. This antenna has a diameter of λ/9 and a height of less than λ/500. The measured gain and radiation efficiency are, respectively, 0dBi and 67%. These figures include the loss of the balun.

7.5 Wideband Array of Coupled Quarter-Wavelength Slot Antenna

A new approach in enhancing the bandwidth of a quarter-wavelength slot antenna is presented. The quarter-wavelength slot antenna design is based on a basic λ/2 slot antenna concept. In this design, several parasitic slot element are used to increase the bandwidth. The dimension and location of each element were determined by measuring the current distribution on the ground plane using Ansoft HFSS full wave simulator. Another approach used to improve the bandwidth is to use the effect of the coupling between the additional microstrip feed line and the driving element. The designed antenna was then fabricated measured in the Radiation laboratory at the University of Michigan. This antenna was fabricated on a FR-4 substrate with a dielectric constant of 4.4 and a loss tangent of 0.02. This antenna provides a fabricated bandwidth of 1.14:1. The measured reflection coefficient showed a good agreement with the simulation result.

For future work, since the new 700MHz band is from 698MHz to 806MHz, increasing the bandwidth of the presented λ/4 slot antenna is highly recommended. One technique to increase the bandwidth is to add more parasitic slot elements to increase the bandwidth to 800MHz. However, increasing the number of the parasitic elements increases the parameters when it comes to determine the location and dimensions of each element. In addition, adding more parasitic

elements affects the coupling between the driving slot element and the parasitics. Another technique could be investigated is the off-centered microstrip feed line technique. By applying this technique, the bandwidth of the slot antenna will be increased, the number of parasitic elements can be reduced and, the overall size of the antenna can be reduced as well.

References

[1] S. D. IIcev, "Code division multiple access (CMDA) applicable for mobile satellite communications," Control and communications (SIBCON) International Siberian Conference, pp. 224-227, Sept. 2011.

[2] W. G. Teich, and M. Seidi, "Code division multiple access communications: multiuser detection based on a recurrent neural network structure," Spread Spectrum Techniques and Applications Proceeding, vol. 3, pp. 979-984, Sept. 1996.

[3] P. Jung, and B. Steiner, "A joint detection CDMA mobile radio system concept developed within cost 231," IEEE 45th, Vehicular Technology Conference, vol. 1, pp. 469-473, Jul. 1995.

[4] Axelsson, R. J. Sune, "Noise Radar For Range/Doppler Processing and Digital Beamforming Using Low-Bit ADC," IEEE Trans. on Geoscience and Remote Sensing, vol. 41, no. 12, pp. 2703-2720, Dec 2003.

[5] R. Stephan, and H. Loele, "Theoretical and Practical Characterization of a Broadband Random Noise Radar," Microwave Symposium Dig. 2000 IEEE MTT-S International, vol. 3, pp. 1555-1558, June 2000.

[6] R. M. Naryanan, Y. Xu, P. D. Hoffmeyer, and J. O. Curtis, "Design, performance, and applications of a coherent ultra-wideband random noise radar," Opt. Eng., vol. 37, no. 6, pp. 1855–1869, June 1998.

[7] D. S. Garmatyuk and R. M. Narayanan, "Ultra-wideband continuous-wave random noise arc-SAR," IEEE Trans. Geosci Remote Sensing, vol. 40, pp. 2543–2552, Dec. 2002.

[8] X. Xu and R. M. Narayanan, "FOPEN SAR imaging UWB step-frequency and random noise waveforms," IEEE Trans. Aerosp. Electron. Syst., vol. 37, pp. 1287–1300, Oct. 2001.

[9] D. C. Bell and R. M. Narayanan, "ISAR imaging using a coherent ultra-wideband random noise radar system," Opt. Eng., vol. 40, no. 11, pp. 2612–2622, Nov. 2001.

[10] S. Kidera, T. Sakamoto, and T. Sato, "High-resolution 3-D imaging algorithm with an envelope of modified spheres for UWB through-the-wall radars," IEEE Trans. Antennas and Propagation, vol. 57, no. 11, pp. 3520-3529, Sept. 2009.

[11] V. Venkatasubramanian, H. Leung, and Xiaoxiang Liu, "Chaos UWB radar for through-the-wall imaging," IEEE Trans. Image Processing, vol. 18, no. 6, pp. 1255-1265, April 2009.

[12] D. D. Ferris, Jr. and N. C. Currie, "A survey of current technologies for through-the-wall surveillance (TWS)," Proc. SPIE , vol. 3577, pp. 62–72, Jan. 1999.

[13] M. Dehmollaian and K. Sarabandi, "Refocusing through building walls using synthetic aperture radar," IEEE Trans. Geosci. Remote Sens.,vol. 46, no. 6, pp. 1589–1599, Jun. 2008.

[14] J. Tatoian, G. Franceschetti, H. Lackner, and G. Gibbs, "Through-the-wall impulse SAR experiments," presented at the IEEE Int. Symp. Antennas and Propagation and USNC/U Nat. Radio Science Meeting, Washington, DC, Jul. 3–8, 2005.

[15] T. Kaiser, E. F. Zheng, and E. Dimitrov, "An overview of ultra-wide-band systems with MIMO," Proc. IEEE, vol. 97, no. 2, pp. 285-312, Feb. 2009.

[16] T. P. Montoya and G. S. Smith, "Land mine detection using a ground-penetrating radar based on resistively loaded Vee dipoles," IEEE Trans. Antennas and Propagation, vol. 47, no. 12, pp. 1795–1806, Dec. 1999

[17] C. Bruns, P. Leuchtmann, and R. Vah ldieck, "Analysis and simulation of a 1–18-GHz broadband double-ridged horn antenna," IEEE Trans. Electromagn. Compatibil., vol. 45, no. 1, pp. 55–60, Feb. 2003.

[18] Hans Schantz, "The art and science of Ultra-wideband Antennas," Norwood, Artech House, INC, 2005.

[19] http://www.ecosurveys.co.uk/ground-penetrating-radar.html

[20] http://www.usradar.com/about-us

[21] Klaus Knödel, Gerhard Lange, and Hans-Jürgen Voigt, "Environmental Geology," Springer.

[22] J. Feigin, R. Roberts, R. Parrillo, J. Rudy, A. Schutz, and J. Thomas, "Noise and interference reduction in air-launched antennas used for GPR evaluation of roads and bridges," Geophysical Survey Systems Incorporated. Salem, NH.

[23] Chi-Chih Chen, Kishore Rama Rao, and R. Lee, "A new ultrawide-bandwidth dielectric-rod antenna for ground –penetrating radar applications," IEEE Trans., Antennas and Propagation, vol. 51, no. 3, pp. 371-377, March 2003.

[24] A. R. Von Hipple, "Dielectric Materials and Applications," NewYork, MIT Press, 1954.

[25] P. Cao, Y Huang and J Zhang, " A UWB monopole antenna for GPR Applications," 6th European Conference, Antennas and Propagation (EUCAP), pp. 2837-2840, March 2012.

[26] I. Hertl and M. Strycek, "UWB antennas for ground penetrating radar application," 19th International Conference on Applied Electromagnetics and Communications, pp. 1-4, Dubrovnik, 24-26 Sept. 2007.

[27] A. S. Turk, D. A. Sahinkaya, H. Nazli, and M. Sezgin, “Investigation of convenient antenna designs for ultra-wide band GPR systems,” 4th International Workshop on Advanced Ground Penetrating Radar, pp. 192-196, Naples, 27-29 June 2007.

[28] https://gtechmini.wordpress.com/multimodal-essays/miniaturization-of-cell-phones/

[29] H. A. Wheeler, “Fundamental limitations of small antennas,”Proc. IRE, vol. 35, pp. 1479–1484, Dec. 1947.

[30] R. Azadegan and K. Sarabandi, “A Novel Approach for Miniaturization of Slot Antennas,” IEEE Transactions. Antennas and Propagation, vol. 51, no. 3, pp. 421 – 429, March 2003.

[31] L. J. Chu, “Physical limitations of omni-directional antennas,” J. Appl. Phys., vol. 19, pp. 1163–1175, Dec. 1948.

[32] H. A. Wheeler, “Small antennas,” IEEE Trans. Antennas and Propagation., vol. AP–23, pp. 462–469, July 1975.

[33] Http://www.fcc.gov/encyclopedia/700-mhz-spectrum

[34] R. R. Harrington, “Effect of Antenna Size on Gain, Bandwidth and Efficiency,” J. Res. Natl. Bur. Stand. D. Radio Propag., vol. 64D, no. 1, pp. 1-12, 1960.

[35] N. Behdad and K. Sarabandi, "A compact antenna for ultrawide-band applications," IEEE Transactions on Antennas and Propagation, vol. 53, no. 7, pp. 2185-2192, July 2005.

[36] A. Elsherbini and K. Sarabandi, "Compact high-isolation directive UWB transmit/receive antenna pair for radar applications," Antennas and Propagation Society International Symposium, 2009. AP-S 2009, June 2009.

[37] Nader Behdad, High-performance, Multi-functional, and miniaturized integrated antennas, Ph.D. Thesis. University of Michigan 2006.

[38] Y. Yoshimura, " A microstripline slot antenna," IEEE Trans. Microwave Theory Tech., vol. MTT-20, pp. 760–762, Nov. 1972.

[39] M. Kahrizi, T. Sarkar, and Z. Maricevic, "Analysis of a wide radiating slot in the ground plane of a microstrip line," IEEE Trans. Microwave Theory Tech., vol. 41, pp. 29–37, Jan. 1993.

[40] J. Sze and K. Wong, "Bandwidth enhancement of a microstrip-line-fed printed wide-slot antenna," IEEE Trans. Antennas and Propagation, vol. 49, pp. 1020–1024, Jul. 2001.

[41] H. G. Booker, "Slot Aerials and Their Relation to Complementary Wire Aerials," J. Inst. Elect. Eng., part III A, pp. 620–626, 1946.

[42] C. Balanis, *Antenna Theory analysis and design*, A John Wiley & Sons, Inc. 2005.

[43] N. Behdad and K. Sarabandi, "A Wide-band slot antenna design employing a fictitious short circuit concept," IEEE Trans. AP, vol. 53, no. 1, pp. 475-482, Jan 2005.

[44] A. Buerkle, K. Sarabandi and H. Mosallaei, "Compact slot and dielectric antenna with dual-resonance, broadband characteristics," IEEE Trans. AP, vol. 53, no. 3, pp. 1020-1027, March 2005.

[45] A. Kishk, Y. Yin, and A. Glisson, "Conical dielectric resonator antennas for wide-band applications," IEEE Trans. Antennas and Propagation, vol. 50, no. 4, pp. 469–474, Apr. 2002.

[46] R. Kumar Mongia and A. Ittipiboon, "Theoretical and experimental investigations on rectangular dielectric resonator antennas," IEEE Trans. Antennas and Propagation, vol. 45, pp. 1348–1356, Sep. 1997.

[47] A. Ittipiboon, R. Kumar Mongia, Y. M. M. Antar, P. Bhartia, and M. Cuhaci, "Aperture fed rectangular and triangular dielectric resonators for use as magnetic dipole antennas," Electronics Letters, vol. 29, pp. 2001–2002, Nov. 1993.

[48] J. Shin, A. Kishk, and A. Glisson, “Analysis of rectangular dielectric resonator antennas excited through a slot over a finite ground plane,” Antennas and Propagation Society International Symposium, vol. 4, pp.2076–2079, July 2000.

[49] T. Morioka, S. Araki and K. Hirasawa, “Slot antenna with parasitic element for dual band operation,” Electronincs Letters, vol. 33, no. 25, pp. 2093-2094, December 1997.

[50] N. Behdad, and K. Sarabandi, “Bandwidth Enhancement and Further Size Reduction of a Class of Miniaturized Slot Antennas,” IEEE Transactions on Antennas and Propagation, vol. 52, no. 8, pp. 1928-1935, August 2004.

[51] I. Bahl, P. Bhartia and S. Stuchly, "Microstrip antennas covered with a dielectric layer," Antenna and Propagation Society International Symposium, vol. 18, pp. 589-592, June 1980.

[52] A. Bhattacharyya, “Effects of dielectric superstrate on patch antennas,” Electron. Lett. vol. 24, no. 6, pp. 356-358, March 1988.

[53] A. Buerkle and K. Sarabandi, "A wideband Circulary Polarized, magnetodielectric resonator antenna," IEEE Trans. AP, vol. 53, no. 11, pp. 3436-3442, November 2005.

[54] Islam, R.; Adve, R., “Beam-forming by mutual coupling effects of parasitic elements in antenna arrays,” Antennas and Propagation Society International Symposium, vol. 1, pp. 126-129, 2002.

[55] Kojiya, T.; Kuwahara, Y., “Improvement of gain of the phased array antenna by the parasitic elements,” Antennas and Propagation Society International Symposium, vol. 3, pp. 812-815, July 2001.

[56] Collin, R.E., Antennas and Radiowave Propagation, McGraw-Hill Book Company, 1985.

[57] R. C. Hansen, “Fundamental limitations in antennas,” Proc IEEE, vol. 69, pp. 170–182, Feb. 1981.

[58] J. Rashed and C. T. Tai, “A new class of Resonant antennas,” IEEE Trans. Antennas and Propagation. , vol. 39, pp. 1428–1430, Sept. 1991.

[59] H. Nakano, H. Tagami, A. Yoshizawa, and J. Yamauchi, “Shortening ratios of modified dipole antennas,” IEEE Trans. Antennas and Propagation, vol. 32, pp. 385-386, 1984.

[60] J. M. Kim, J. G. Yook, W. Y. Song, Y. J. Yoon, J. Y. Park, and H. K. Park, “Compact meander-type slot antennas,” in Proc. Antennas and Propagation. Soc. Int. Symposium., AP-S. Dig. , vol. 2, pp. 724–727, Boston, MA, July 2001.

[61] Jung-Min Kim, Kun-Wook Kim, Jong-Gwan Yook and Han-Kyu Park, “Compact stripline-fed meander slot antenna,” Electronics Letters, vol. 37 , pp. 995-996, August 2001.

[62] H. Y. Wang, and M. J. Lancaster, “Aperture coupled thin film superconductor meander antennas,” IEEE Trans. Antennas and Propagations. Vol. 47, pp. 829-836, Oct. 1998.

[63] Sarabandi, K., and R. Azadegan, “Design of an Efficient Miniaturized UHF Planar Antenna,” IEEE Transactions on Antennas and Propagation, vol. 51, no. 6, pp. 1270 – 1276, June 2003.

[64] Wonbin Hong and K. Sarabandi, "Low Profile Miniaturized Planar Antenna with Omnidirectional Vertically Polarized Radiation," IEEE Trans. AP, vol. 56, no. 6, pp. 1533-1540, June 2008.

[65] J. D. Kraus and R. J. Marhefka,”Antennas,” (McGraw Hill, 3rd edn.)

[66] Yong-Xin Guo, Z. Y. Zhang, L. C. Ong and M. Y. W. Chia, “A Novel LTCC Miniaturized Dualband Balun,” IEEE Microwave and wireless component Letters, vol. 16, pp. 143-145 March 2006.

[67] S. I. Latif, L. Shafai, and S.K. Sharma, "Bandwidth enhancement and size reduction of microstrip slot antennas," IEEE Trans. Antennas and Propagation, vol. 53, pp. 994–1003, March 2005.

[68] S. C. K. Ko and R. D. Murch, "A diversity antenna for external mounting on wireless handsets," IEEE Trans. Antennas and Propagation, vol. 49, pp. 840–842, May 2001.

[69] D. Pozar, "Microwave engineering," 4th edition, John Wiley & Sons, Inc.